International Journal of Precision Engineering and Manufacturing (2022) 23:1477–1502
https://doi.org/10.1007/s12541-022-00717-z

Online ISSN 2005-4602
Print ISSN 2234-7593

REVIEW

Fabrication Methods for Microscale 3D Structures on Silicon Carbide

Younghak Cho[1] · Jihong Hwang[1] · Min-Soo Park[1] · Bo Hyun Kim[2]

Received: 20 April 2022 / Revised: 11 July 2022 / Accepted: 5 September 2022 / Published online: 12 October 2022

Abstract
Silicon carbide (SiC) is an attractive material for many industrial applications, such as semiconductors, electronic power devices, and optical and mechanical devices, owing to its wide bandgap, high thermal and wear resistance, and chemical inertness. Although SiC has superior properties, fabricating micro-features on SiC is very expensive and time-consuming. Many studies have introduced various fabrication methods utilizing physical, chemical, and thermal principles to remove SiC material. This paper reviews the state-of-the-art processes applicable for fabricating micro-3D structures on SiC, including etching, mechanical, thermal, and additive processes. The advantages and limitations of these processes are also discussed to guide the selection of processes suitable for SiC.

Keywords Silicon carbide · Fabrication · 3D structure · Micro scale

1 Introduction

Silicon carbide (SiC) is a promising material for semiconductor and microelectronic devices as well as mechanical components and biomedical applications. Compared to silicon, SiC has a wider band gap and ten-fold higher dielectric breakdown strength, which allow for a high breakdown voltage of over 600 V. Moreover, it has high thermal conductivity and resistance to high temperatures, which are properties required for high-power electronic devices. These advantages make SiC a potential material to replace silicon- and germanium-based wafers. SiC exhibits good mechanical, thermal, and chemical properties. Thus, SiC is an excellent material for mechanical components that require a high wear resistance. SiC exhibits higher hardness than other ceramic materials. The hardness of SiC is approximately 22 GPa HV, which is higher than that of alumina (15.7 GPa), silicon nitride (13.9 GPa), and zirconia (12.3 GPa). Because SiC has high chemical stability and low thermal distortion at high temperatures, it can be used in furnace heating elements, wafer fixtures, and showerheads in chemical vapor deposition (CVD) processes. In addition, the chemical inertness and biocompatibility of SiC allow for it to be used in biomedical applications.

SiC is an attractive and preferred material compared to silicon wafers or other ceramic materials. However, machining SiC remains challenging owing to its high hardness, brittleness, and chemical resistance. The recent demand for machining processing is not limited to the grinding or polishing of SiC wafers, but also to the fabrication of various micro-features such as holes, grooves, channels, or complex 3D microstructures. The applications of fabricating 3D features include SiC-based power micro-electromechanical systems (MEMS), micro-holes of CVD components, aspherical SiC micro-mold cores for glass lens arrays, SiC wafer dicing, and ultra-precision mirror surfaces for space telescopes.

Each of the fabrication methods for SiC is based on different physical, chemical, or hybrid principles and has unique characteristics. Therefore, the fabrication method should be carefully selected based on the features required for various applications. This paper reviews the state-of-the-art 3D fabrication methods for SiC. The scope of this review is confined to the process techniques for high-purity SiC, such as single-crystalline SiC and CVD or sintered SiC, although there are many SiC composites. Section 2 introduces the different types of SiC materials and their applications. Section 3 presents SiC fabrication methods, which are classified into chemical and dry etching and mechanical, thermal, and

✉ Bo Hyun Kim
bhkim@ssu.ac.kr

[1] Department of Mechanical System Design Engineering, Seoul National University of Science and Technology, 232 Gongneung-Ro, Nowon-Gu, Seoul 01811, Republic of Korea

[2] School of Mechanical Engineering, Soongsil University, 369 Sangdo-Ro, Dongjak-Gu, Seoul 06978, Republic of Korea

additive processes. This review provides a guide for selecting methods that are suitable for the fabrication of 3D structures on SiC.

2 Materials and Applications

2.1 SiC Materials

SiC is an attractive material with a large number of atomic configurations in the amorphous, polycrystalline (sintered and CVD), and monocrystalline form/phase; its structure and properties are dependent on the preparation conditions.

Amorphous SiC (a-SiC) can be easily prepared through low-temperature (400 °C) CVD from a SiH_4/CH_4 gas mixture [1], and hydrogenated amorphous SiC (a-Si_xC_{1-x}:H) is used as an optoelectronic material (such as for visible light-emitting diodes (LEDs) and emitters for high-speed bipolar transistors (HSBTs)) owing to its optical bandgap, which can be controlled from 1.8 to 3 eV by changing the Si–C content [2]. Polycrystalline SiC can be grown on a wide variety of substrates such as Si, Si_3N_4, and SiO_2 at higher temperatures (500–1200 °C) than a-SiC, and various processes exist compared to that for monocrystalline epitaxial film growth [3]. Polycrystalline SiC consists of several small crystalline regions (called grains or crystallites) bonded together by crystallographically defective regions (called grain boundaries). The grains formed using CVD processes are sensitive to several parameters, such as the temperature, deposition rate, dopant concentration, pressure, and impurity concentration [3]. On the other hand, sintered α-SiC is produced by initially mixing fine (sub-micron) and pure SiC powder with non-oxide sintering aids [4]. Boron and carbon are used as sintering aids to achieve improved densification during sintering, which is typically conducted at a temperature of approximately 2500 °C. The resulting structure consists predominantly of fine equiaxed grains of the 6H polytype, although a small amount of free carbon and isolated B_4C grains may be present.

Single-crystalline SiC (c-SiC) exists in more than 250 crystalline forms called polytypes. The crystal structures vary in the different stacking sequences of the Si–C double layers, where each Si is surrounded by four C atoms and vice versa (Fig. 1) [5]. The most common polytypes of SiC are 2H, 3C, 4H, 6H, and 15R; however, the majority of research and development has focused on only three types: 3C, 6H, and 4H. The numbers refer to the number of layers in the unit cell, and the letter designates the crystal structure, where C, H, and R denote cubic, hexagonal, and rhombohedral structures, respectively [6]. 4H-SiC is preferred for power electronic devices primarily because of its superior material properties such as high carrier mobility [7]. Its bandgap is 3.27 eV at room temperature (Fig. 1b), which dramatically reduces the number of electron–hole pairs formed from thermal activation across the bandgap and allows the high-temperature operation of SiC electronic devices. 3C-SiC is more common for MEMS-based sensors because it can be easily grown on Si wafers, which reduces the overall wafer cost [8]. 6H-SiC has been used for UV photodiodes as well as solid-state lighting (LEDs) owing to its similar lattice constant to that of the GaN family of alloys [2].

2.2 Applications

SiC has attracted considerable attention because of its superior characteristics, such as a wide bandgap, high breakdown electric field, excellent oxidation resistance, low density, high melting point, high thermal conductivity, high chemical inertness, chemical stability, good microwave absorbing ability, and high mechanical strength [9, 10].

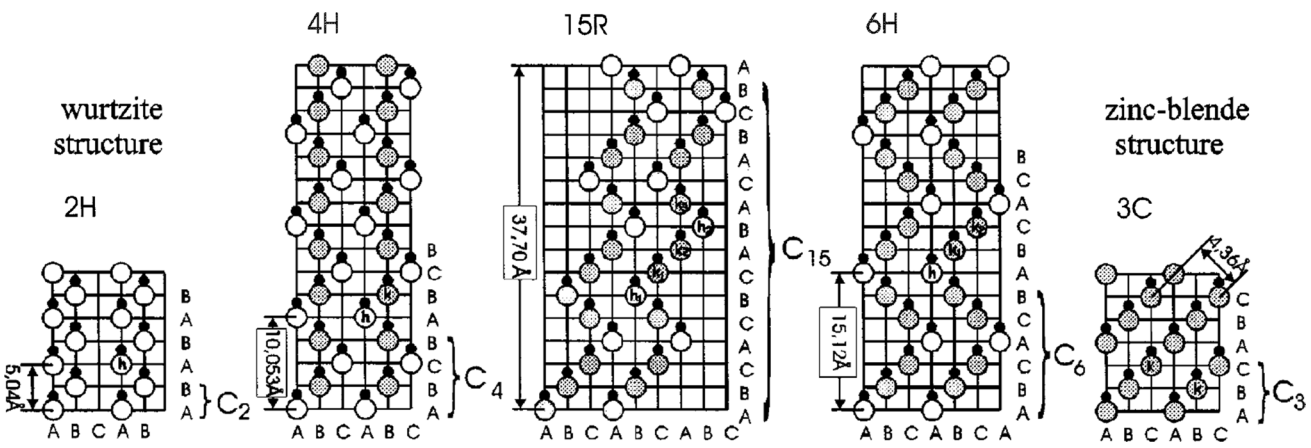

Fig. 1 Crystallographic stacking sequences of Si–C double layers. Reproduced with permission from Ref. [5]

Table 1 lists the basic properties of several semiconductor materials [5]. The data indicate that SiC can be used for applications in harsh environments, such as high radiation exposure, operation at high temperatures, and in corrosive media [11]. Specifically, the basic properties of SiC provide several advantages for electronic devices compared to Si [12].

First, the limit operation temperature for SiC devices (> 400 °C) is higher than that of Si (< 200 °C) owing to the wide bandgap, which can ensure the long-term reliability of devices that operate at high temperatures. Therefore, SiC can be used as a sensing device in chemical production and as a high-temperature gas sensor in turbine or engine testing industries to detect flammable and combustible gases in harsh, high-temperature, and corrosive environments [13]. Second, SiC devices can sustain much higher voltages than Si devices; thus, their size can be reduced because of the higher critical breakdown electrical field of SiC (ten times that of Si). This means that SiC is valuable for the development of electric vehicles, solar power inverters, energy storage converters, and sensor systems [14]. Third, SiC devices can conduct heat much more effectively because of the higher thermal conductivity of SiC (three times that of Si). Therefore, SiC can be used for thermal management applications in semiconductors and electronic devices and for high-heat-load applications in rapid thermal processing (RTP) and plasma etching systems, radio frequency (RF) heated susceptors, synchrotron and high-energy laser mirrors, and optics molds [15].

SiC has been used as a versatile material for biosensors [3], biomedical applications [16], and bioimaging [17]. The chemical inertness of SiC leads to a high resistance to corrosion in harsh environments such as bodily fluids. Its high elastic modulus and low friction coefficient render SiC an ideal material for smart implants [18] and in vivo biosensors [3]. As a representative biomedical application, SiC has been used as a hard coating material for non-fouling coronary heart stents [19].

A previous review described recent progress in SiC-based nano-architectures covering their structure, properties, and defects with respect to multidisciplinary applications such as photocatalysis, membrane technology, field-emission transistors, nano-electronics, biosensors, medical implants, and photothermal, photodynamic, and regenerative medicine (Fig. 2) [9]. Several other reviews have focused on the properties of SiC, including the piezoresistive effect of SiC for MEMS [20], next-generation nanoelectronics for environmental monitoring [21], electronic devices [22], and energy harvesting [23].

3 Fabrication Methods

3.1 Etching

Owing to its extreme mechanical and chemical stability and robustness, monocrystalline (single-crystal) SiC is stable in all known aqueous etching solutions [10]. In other words, SiC is resistant to almost all chemicals except for molten KOH above 600 °C [24] and alkaline solutions of $K_3Fe(CN)_6$ above 100 °C [25]. Therefore, it is very difficult to etch single-crystal SiC substrates to fabricate micro/nanostructures. Recently, several hybrid approaches have been reported, such as electrochemical etching [26, 27], metal-assisted hybrid etching [28], and photoelectrochemical etching [29, 30].

Plasma-based dry etching, which is usually employed in the SiC etching industry, is considered the only practical way to pattern SiC owing to the high bonding energy of the SiC material [31]. Among the dry etching techniques employed to date, inductively coupled plasma (ICP) etching can provide a higher plasma density for an appropriately high etching rate and less sample surface damage than other dry etching methods [32]. Because ICP systems have several advantages, such as simple operation, easy automatic control, and availability for large-area substrate etching, they

Table 1 Comparison of basic properties of several semiconductor materials [5]

Property/material	4H-SiC	6H-Sic	Si	GaAs
Thermal conductivity (W/cm K)	4.9	4.9	1.3	0.5
Bandgap (eV)	3.2	3.0	1.12	1.42
Intrinsic material transparent	Yes	Yes	No	No
Available doping	n, p	n, p	n, p	n, p
Saturated electron drift velocity (10^7 m/s)	2.0	2.0	1.0	2.0
Electron mobility (cm^2/Vs)	1000	600	1450	8500
Critical breakdown electrical field (MV/cm)	3	3.2	0.3	0.6
Lattice constant (*a*)	3.073	3.081	3.84	4.00
Lattice mismatch with GaN (%)	3.8	3.5	− 17	− 22
Thermal expansion mismatch with GaN (%)	− 0.11	− 0.12	− 0.17	0.11

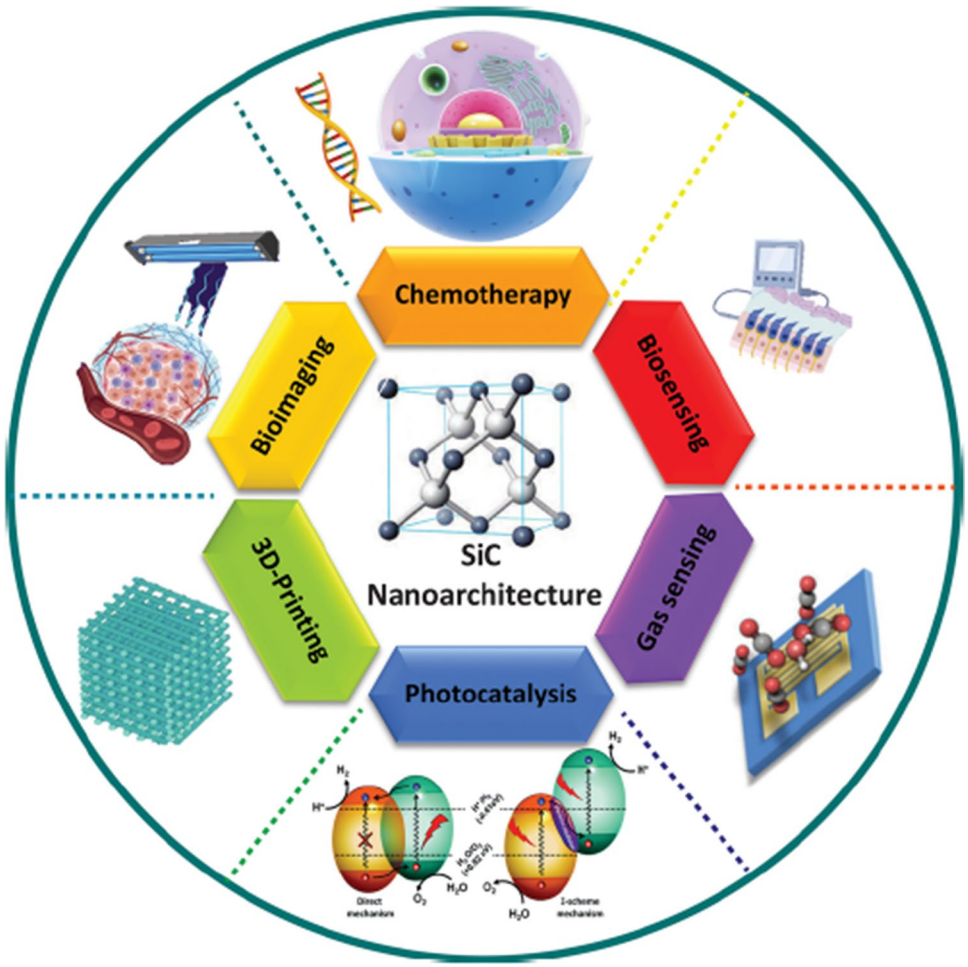

Fig. 2 SiC nano-architectures for diverse applications. Reproduced with permission from Ref. [9]

have been widely used in the fabrication of SiC devices [33–38].

In this section, dry and wet etching of SiC are reviewed, including conventional wet etching in aqueous solutions, electrochemical etching, and photoelectrochemical etching.

3.1.1 Conventional Wet Etching

Wet chemical etching is an attractive approach owing to its low process cost and low process-induced damage [10]. However, the large bandgap and low-lying valence band edge make direct chemical etching of SiC nearly impossible, except for molten KOH etching. The advantages of molten KOH etching are widely acknowledged, and it has been used to detect crystalline defects in SiC as etch pits in crystal growth research [2, 24, 39].

Katsuno et al. investigated the etching mechanism of SiC single crystals in molten KOH [24]. The etching rate was significantly enhanced by the presence of oxygen in the etching environment. Fukunaga et al. developed anisotropic wet chemical etching of single-crystalline hexagonal SiC using molten KOH for SiC bulk micromachining [39]. The (0001)Si and (000-1)C faces of the 6H-SiC substrates were used. The etching rates of the (0001)Si and (000-1)C faces at 490 °C were evaluated to be 37 nm/min and 3.1 μm/min, respectively, indicating that etching of the (0001)Si face was almost 100 times slower than that of the (000-1)C face (Fig. 3).

On the other hand, single-crystalline SiC can be chemically etched in aqueous etchants by first making it amorphous despite its inertness. Henkel et al. [40] implanted an SiC sample using high-dose Xe^+ ions and etched it in a boiling 1:1 mixture of HF and HNO_3. Alok and Baliga [41] demonstrated highly anisotropic etching by producing trenches of 0.3–0.8 μm on a 6H-SiC sample using ion implantation. In addition, they showed that deeper trenches could be obtained by repeating the implantation/etching steps using platinum as the masking material.

3.1.2 Electrochemical Etching

Van Dorp et al. comprehensively described the electrochemical etching of 4H-SiC in an HF solution of pH 3, considering the surface reactions, kinetics, and mass transport [42].

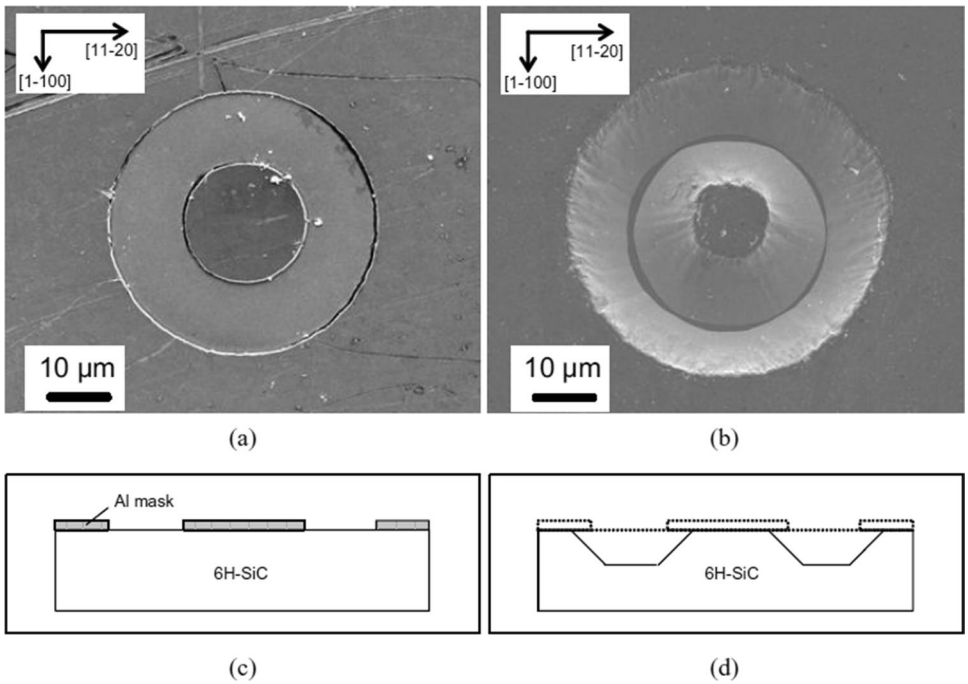

Fig. 3 SEM images of the (000-1)C surface before and after molten KOH etching at 470 °C for 4 min. **a** Bird's-eye view before etching. **b** Bird's-eye view after etching. **c** Cross-section schematic before etching. **d** Cross-section schematic after etching. Reprinted with permission from Ref. [39]

A uniform longitudinal distribution of SiC mesopores on the 4H-SiC substrate with a thin cap and transition layer was first fabricated by pulsed electrochemical etching [26]. Chen et al. successfully fabricated gourd-shaped nanowires on 4H-SiC using anodic oxidation with a pulsed voltage in a solution of $HF:C_2H_5OH:H_2O_2 = 3:6:1$ [43].

A hybrid anodic and metal-assisted chemical etching method was proposed to fabricate SiC nanowires based on wet etching at room temperature and atmospheric pressure. The voltage required to create holes in the anodic etching of SiC was reduced to less than 10 V using Pt metal, which played two key roles in the process: it acted as a catalyst to produce hole carriers and introduced band bending in SiC to accumulate sufficient holes for etching [28].

The active substance of fluorine is indispensable in the above-mentioned cases; however, it poses a severe threat to both humans and the environment. Zhan et al. proposed a microtool-based HF-free wet etching method (electrolytic plasma etching) to fabricate SiC microstructures [27]. Semiconductor 4H-SiC (0001) was etched using electrolytic plasma etching in an HF-free aqueous solution (Fig. 4).

3.1.3 Photoelectrochemical Etching

Zhao et al. reported a micromachining process technology for the fabrication of MEMS on SiC [30]. Suspended microstructures of single-crystal SiC were fabricated using a dopant-selective photoelectrochemical etching process, which allowed the undercutting of the p-SiC layer by rapid lateral etching of the underlying n-SiC substrate. Figure 5 shows scanning electron microscopy (SEM) images of single-crystal SiC MEMS structures fabricated using

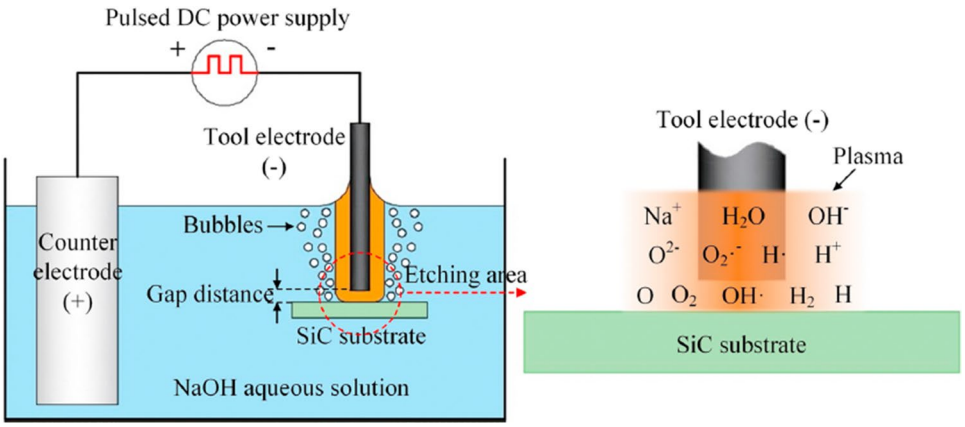

Fig. 4 Schematic diagram of tool-based electrolytic plasma etching of 4H-SiC for micro/nanostructure fabrication. Reprinted with permission from Ref. [27]

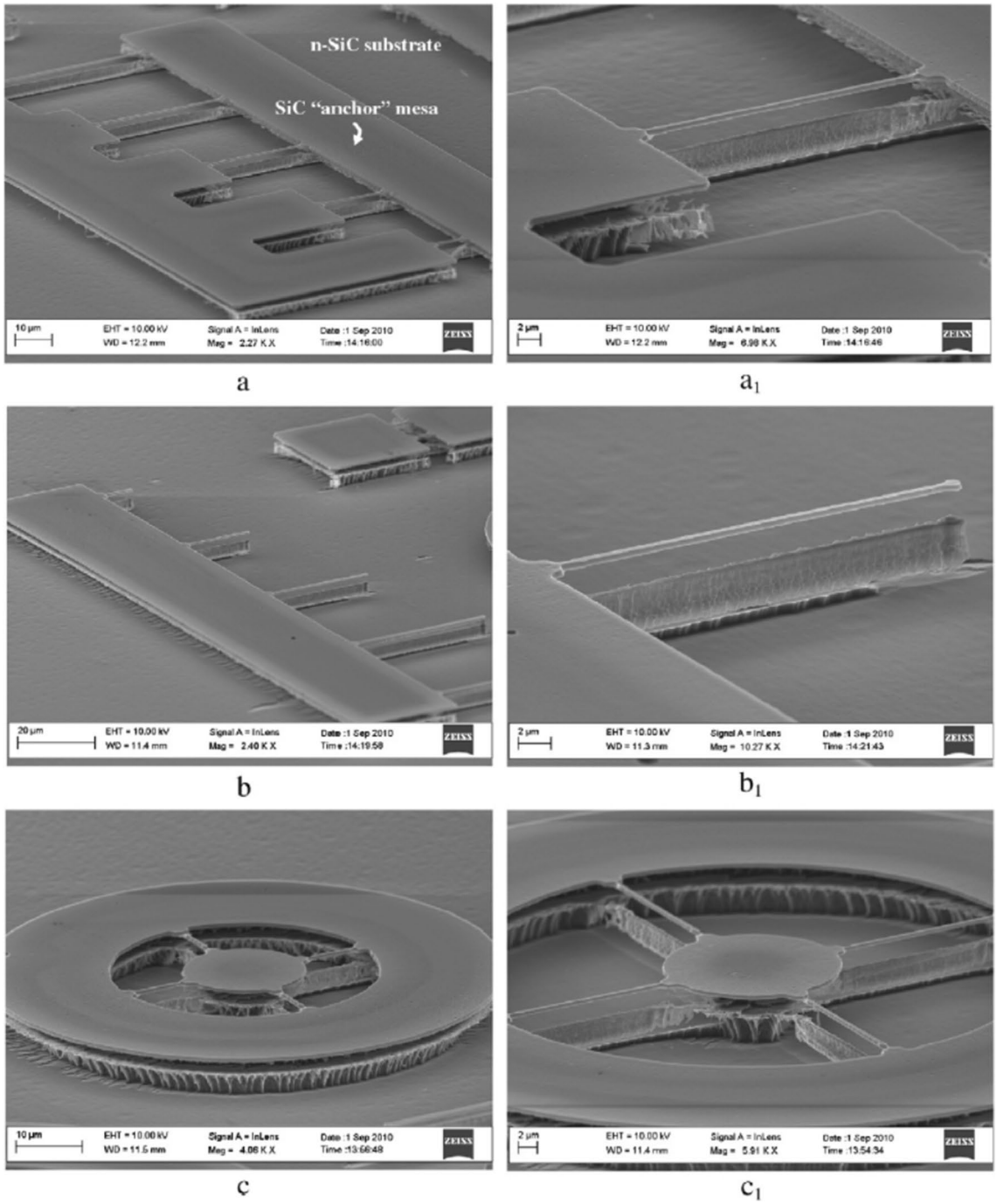

Fig. 5 **a**–**c** SEM micrographs of single-crystal SiC MEMS structures fabricated using dopant-selective photoelectrochemical etching, and **a1**–**c1** close-up images of the microstructures. Reprinted with permission from Ref. [30]

dopant-selective photoelectrochemical etching. Photoelectrochemical etching of highly doped n-type 4H-SiC in dilute hydrofluoric acid along different crystallographic orientations under low-voltage and/or low-current conditions has also been studied [29]. Leitgeb et al. proposed metal-assisted photochemical etching of 4H-SiC as a reliable and simple technique for the generation of uniform and highly porous 4H-SiC layers [44]. They concluded that UV light irradiation and an oxidizing agent were important for the formation of the porous layer.

3.1.4 Dry Etching

As mentioned above, ICP-reactive ion etching (RIE) is the only technique that enables reproducible etching processes with high anisotropy, selectivity, and etching rates. Therefore, many studies have been conducted on ICP-RIE for SiC etching, and a review of ICP-RIE for SiC has recently been published [45]. That review presented the principles of the ICP-RIE method and representative results of SiC etching.

Jiang et al. found that in the ICP etching mechanism of SiC in Cl_2/Ar plasma, the etching regime was affected by the ratio of reactive Cl^- ions to Ar^+ ions, depending on the etching conditions [31]. In addition, they observed that the SiC etching rate increased with a decrease in the substrate temperature. Luna et al. demonstrated deep reactive ion etching (DRIE) of high-aspect-ratio structures in 4H-SiC [35]. They used an electroplated nickel mask and SF_6/O_2 ICP-RIE to realize high aspect ratio trenches with depths of 51–57 µm. Osipov et al. demonstrated an effective method for the formation of deep (30 µm), highly oriented (90° sidewall angle) structures with sub-nanometer surface roughness in SiC [37]. These structures were obtained by dry etching in SF_6/O_2 ICP at increased substrate holder temperatures. As the etching temperature increased, the etching rate increased monotonically up to the moment when other factors became limiting for the etching rate. They also presented the results of an in-depth study of the plasma-chemical etching process of single-crystal SiC in SF_6/O_2 ICP [36]. Choi et al. demonstrated a top-down fabrication technique for nanometer-scale SiC pillars using ICP etching [33]. The etching characteristics of 4H-SiC (0001) were investigated using ICP etching in an SF_6/O_2 plasma to fabricate SiC nanopillars. The etching profile of the SiC nanopillars and the etching rate were controlled by varying the O_2 concentration in the etching gas. The effects of the bias voltage and chamber pressure were investigated using a circular mask pattern of 115 nm.

To investigate the microtrenching effect of ICP etching for single crystal 6H-SiC, SF_6 mixed with O_2 plasma was used as the etching atmosphere [38]. The percentage of O_2 was identified as the most important parameter. The addition of O_2 influenced the effect of the microtrenching owing to the formation of a SiF_xO_y layer, which had a greater tendency to charge than SiC. Sung et al. presented a detailed fabrication method together with validation, discussion, and analysis for state-of-the-art SiC etching of vertical and beveled structures using ICP-RIE for microelectronic applications [46]. Figure 6 shows SEM images of various via-holes formed on a SiC substrate using the optimized parameters for the ICP-RIE technique.

In addition to ICP-RIE, several studies have been conducted using conventional plasma etching techniques. Sano et al. developed a wafer-thinning apparatus with a rectangular raised frame and attempted to thin a SiC wafer using plasma chemical vaporization machining, which involves plasma etching using atmospheric-pressure plasma [47]. Habuka et al. applied chlorine trifluoride (ClF_3) gas as a polycrystalline β-SiC etchant for the first time, studied the chemical reactions, and etched the surface of β-SiC [48]. They also studied the etching rate and etched surface morphology of a polycrystalline β-SiC substrate using 10–100% ClF_3 gas [49]. The surface morphology of single-crystal 4H-SiC etched using ClF_3 gas was studied over a wide temperature range of 570–1570 K at atmospheric pressure in a horizontal cold wall reactor [50].

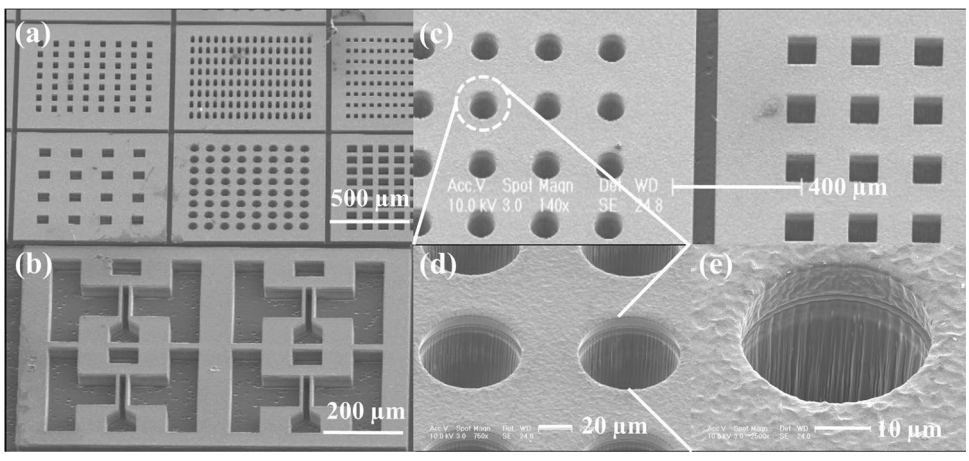

Fig. 6 SEM images of various via-holes formed on SiC substrates using optimized parameters for the ICP-RIE technique. **a** Mask opening widths of 35, 25, 20, 100, 70, and 70 µm (from the top left, row first). **b** Vertically etched SiC with a complicated pattern and a well-etched sidewall profile. **c** Mask opening widths of 70 µm (circular) and 70 µm (square) from left to right. **d** 5× enlargement of the circular pattern. **e** 10× enlargement of the circular pattern. Reprinted with permission from Ref. [46]

3.2 Mechanical Processes

3D structures can be created at the microscale using mechanical processes in which physical forces or impacts are exerted on the target area by tools or accelerated particles. Even though mechanical processes have relatively low precision and productivity compared to lithographic processes, they are advantageous in that complex 3D structures can be fabricated with a high degree of flexibility and at relatively low cost, especially when the part quantity is small. It should be noted, however, that not all mechanical processes are appropriate for the fabrication of microscale 3D structures on high-purity SiC in which crack-free surfaces are required with good dimensional accuracy and surface roughness. Among the various mechanical processes, chip formation and ion beam processes have more often been employed for the fabrication of microscale 3D structures on SiC. Thus, studies from the last two decades applying these processes for the fabrication of microscale 3D structures on high-purity SiC are reviewed here.

3.2.1 Chip Formation Processes

Although SiC is brittle, it can be machined in a ductile regime if the uncut chip thickness is sufficiently small. Machining in the brittle regime is achieved through brittle fracture by crack propagation, whereas machining in the ductile regime is accomplished through material removal by plastic deformation, resulting in smooth surfaces [51–55]. Regarding this phenomenon, it was reasoned that if more energy is needed to propagate a crack than for the plastic yielding of the material, material removal by plastic deformation will prevail [51]. Alternatively, it was reasoned that at nanoscales, in which defects rarely pre-exist and thus stress concentrators leading to crack initiation and fracture are few, plastic deformation by high-pressure phase transformation (HPPT) and/or dislocation nucleation will be more prevalent.

However, it should be noted that to produce a crack-free surface in practice, machining does not need to be carried out completely in the ductile regime. When the ductile and brittle regimes are properly combined, machining can be performed more efficiently without forming cracks on the machined surface. In diamond turning, for example, cracks begin to form along the uncut shoulder when the uncut chip thickness reaches a critical value, as shown in Fig. 7 [56, 57]. In this case, if the depth of the surface damaged by these cracks is smaller than that of the machined surface, the machined surface will be free of cracks. This principle applies not only to diamond turning, but also to grinding and milling.

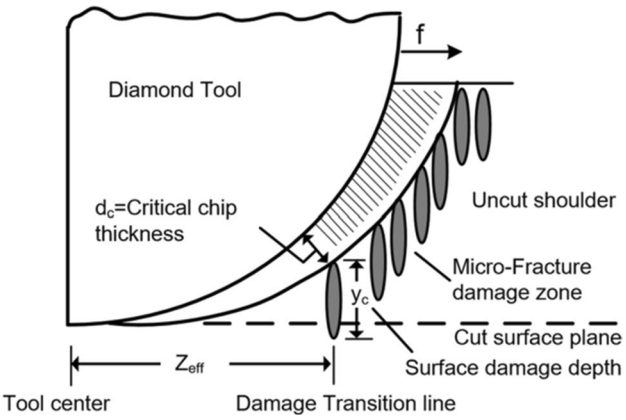

Fig. 7 Schematic cutting model for the critical depth-of-cut [56]

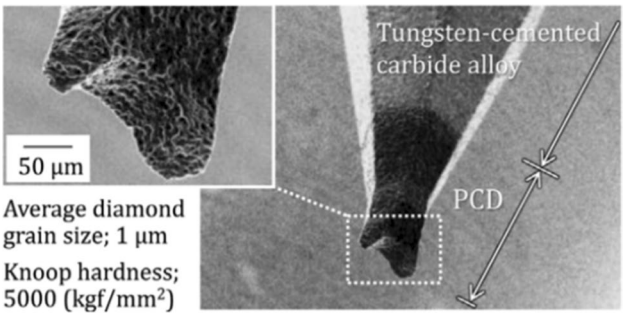

Fig. 8 SEM image of a pencil-shaped PCD end mill [68]

3.2.1.1 Conventional Processes Grinding in the ductile regime has been actively employed for the fabrication of optical elements with 3D convex or concave surfaces. Because crack-free surfaces can be produced by grinding alone, the need for post-processes such as polishing and lapping can be eliminated, and significant time and cost savings can thus be realized. This was enabled by the development of ultra-precision grinding systems with CNC servo controllers. As a result, spherical [58, 59], aspherical [58, 60–62] and freeform surfaces [63–66] have been successfully ground in the ductile regime using cup-shaped, peripheral, or elastic wheels [60, 63] for various types of high-purity SiC materials, including CVD [58, 60–63], monocrystalline [65], polycrystalline [59] and additively manufactured [64] SiC.

However, the grinding methods employed for fabricating optical elements from SiC are limited in the construction of microscale 3D structures with higher complexity. In this regard, a method of using a pencil-shaped polycrystalline diamond (PCD) tool was developed to machine microscale 3D structures. In this case, the tool itself is similar to a micro end mill that has intermittent contact with the workpiece during machining (Fig. 8). However, the material removal mechanism is similar to micro-grinding, in which randomly

distributed diamond abrasives act as hard cutting edges when the tool is rotated, rather than micro-milling. Accordingly, chip loading or adherence onto the tool, which is typically found in micro-grinding, is observed during the cutting of SiC materials. Takesue et al. [67] and Katahira et al. [68] developed a method of conditioning the tool electrochemically and showed that microscale 3D structures such as wells and grooves (Fig. 9) could be machined using this method.

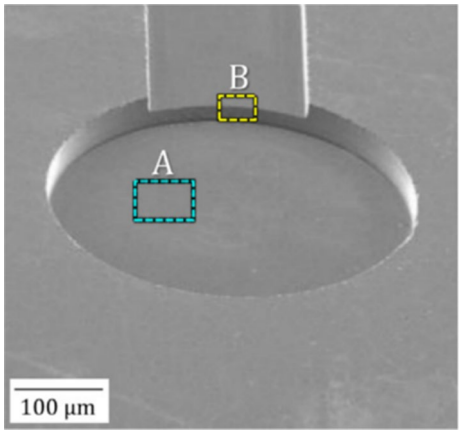

Fig. 9 SEM image of a well-and-groove structure micro-machined on high-purity SiC [68]

In contrast, Suzuki et al. [69] developed micro-milling tools made of binderless nano-polycrystalline diamond (NPCD) using a laser beam (Fig. 10). The developed tools were harder and tougher than those made of single-crystalline diamond, resulting in much higher wear resistance and better surface finishes in SiC machining. Using these tools, a micro-lens array mold with v-grooves made of CVD SiC and single-crystalline SiC could be machined successfully.

Dicing and wire sawing are widely used in the semiconductor industry to cut ingots and wafers. However, these methods can be utilized to machine more complex structures on SiC. Cvetkovic´ et al. [70] conducted experiments to compare the performance of ultra-precision dicing and wire sawing for monocrystalline and polycrystalline SiC ceramics. The results indicated that dicing was better for reducing edge chipping and sidewall roughness but worse for form accuracy than wire sawing.

3.2.1.2 Hybrid Processes Ultrasonic vibration-assisted machining (UVAM) is a hybrid process that combines machining with high-frequency low-amplitude vibrations. UVAM has been employed to machine hard and brittle materials efficiently and has been shown to decrease cutting forces, improve surface quality, and reduce cutting temperatures and tool wear [71]. However, it should be noted that the application of UVAM for SiC has only recently been

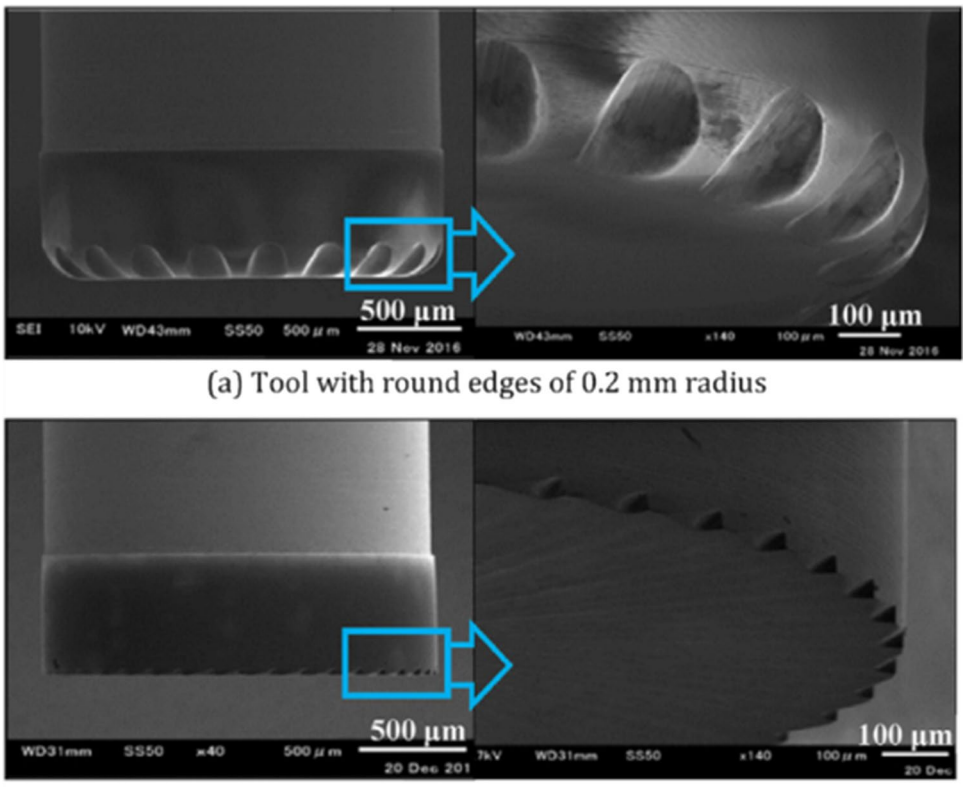

Fig. 10 SEM images of micro-NPCD milling tools fabricated by laser machining [69]

attempted; thus, its potential is not yet fully understood. In this context, Cao et al. [72] conducted an ultrasonic-assisted scratching test of SiC ceramics with a single-crystalline diamond tool to investigate the material removal behavior in UVAM. The results showed that compared to conventional scratching, the critical depth-of-cut and mean groove depth increased in UVAM. When applied to the internal grinding of SiC ceramics, it was found that the grinding forces were considerably reduced, the form accuracy and surface roughness were improved, and grinding cracks occurring on the work surface were considerably restrained. Recent studies on diamond cutting and diamond wire sawing of SiC have shown the effectiveness of elliptical and three-dimensional ultrasonic vibrations rather than one-dimensional vibrations [73, 74]. Furthermore, it was shown that by taking advantage of UVAM, microstructures such as Echelle gratings [75] and pressure sensor diaphragms [76, 77] (Fig. 11) could be successfully machined on SiC.

Laser-assisted machining (LAM) combines a laser beam with machining to increase the ease of machining for hard and brittle materials [78, 79]. In this case, the laser beam is focused onto the region near the cutting zone to locally heat the work materials and thus change their characteristics from brittle to ductile. While LAM is quite popular in the machining of other hard and brittle materials, only a few studies have been reported regarding the LAM of high-purity SiC. In the studies by Patten et al. [80–82], scratch tests were performed on a 4H-SiC wafer using a single-crystalline diamond tool through which an IR laser beam passed. Compared to the conventional method, the results showed that the depth-of-cut was increased by the irradiation of the laser beam for the same applied force, while the specific energy and hardness were decreased. It was also observed that the critical depth-of-cut, or the depth-of-cut at which ductile to brittle transition occurred, was increased with the use of the laser beam [81]. In their simulations, it was found that the machining force decreased significantly as a result of thermal softening [83]. In addition, based on molecular dynamics (MD) simulation results, Meng et al. [84] suggested that the machinability of SiC could be effectively improved by surface modification using a femtosecond laser beam. For example, they showed that when the morphology of the modified layer was a grating structure, the removable amount of SiC could be increased, while the subsurface damage depth was reduced.

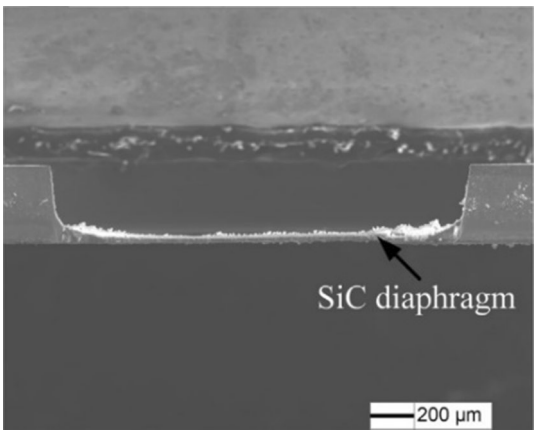

Fig. 11 SEM image of a SiC sensor diaphragm with a thickness of 20.3 μm fabricated by UVAM [77]

Hybrid processes involving chemical reactions have also been developed for SiC machining. Katahira et al. [85] performed micro-mill grinding of CVD SiC using micro-PCD tools with application of an atmospheric-pressure plasma jet. As a result, a high-quality surface with an average roughness (R_a) of 1–2 nm was obtained for a machining distance of up to approximately 3000 mm without the adhesion of contaminating materials on the tool surface. Elemental analysis and wettability tests of the workpiece surfaces indicated the generation of an SiO_2 layer and an increase in hydrophilicity due to the plasma jet irradiation. It was believed that this would facilitate the action of coolant in cooling and removing surface contamination at the tool edge during machining, leading to an improvement in the machining efficiency in SiC micro-grinding (Fig. 12). Chen et al. [86] proposed a method that combined surface modification by an electrolyte jet with material removal by mill grinding for SiC (Fig. 13). In this hybrid process, the electrolyte jet selectively softens the surface by generating a SiO_2 layer, which can be subsequently removed using a soft abrasive tool. The use of

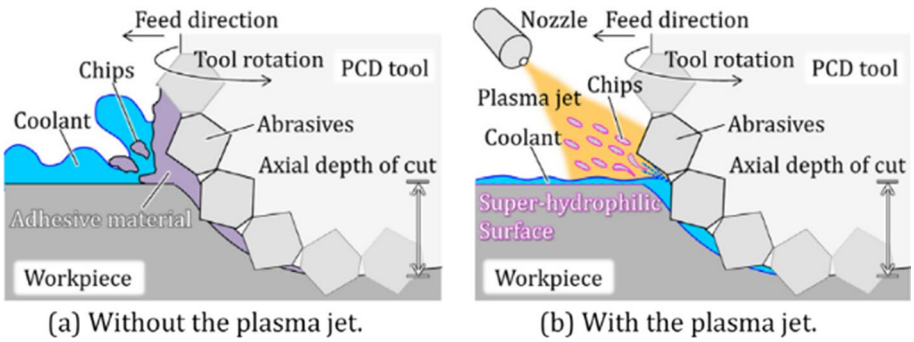

Fig. 12 Schematic of the plasma-jet-assisted cooling mechanism at the interface between the workpiece and the tool edge during PCD micro-mill grinding [85]

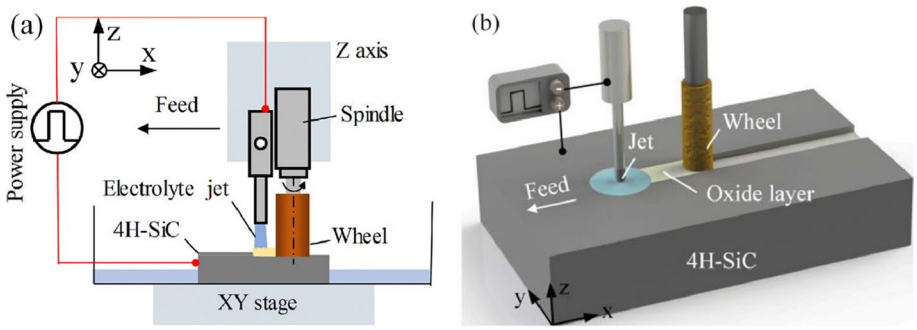

Fig. 13 Schematic of electrolyte jet-assisted grinding [86]

soft abrasives such as Al_2O_3 allows an extremely smooth surface to be obtained with little subsurface damage on a 4H-SiC wafer (Fig. 14). In addition, the material removal rate was significantly increased, while the wear of the soft abrasive tool was substantially reduced compared to that in conventional grinding without the application of an electrolyte jet. This enhancement in grinding efficiency is related to the continuous self-sharpening of the soft abrasive tool as a result of grain fracture occurring when the grinding wheel directly contacts the hard substrate material below the modified layer. It was also suggested that the reduction in the actual grit depth-of-cut for the hard substrate material by the thickness of the modified layer facilitates material removal in the ductile regime.

A new method called ion-implantation-assisted machining has been introduced for nanoscale machining of brittle materials; this method combines surface modification by ion implantation and material removal by diamond machining [87]. Ion-implantation-assisted machining has been shown to enhance machining efficiency and surface quality by increasing the ductile-to-brittle transition depth, reducing the cutting forces, and prolonging the tool life. The feasibility of applying this method to machining 6H-SiC was recently investigated by Tanaka and Shimada [88]. They performed carbon ion implantation to modify the surface structure of monocrystalline 6H-SiC into an amorphous structure. The results of machining experiments conducted on the modified surface revealed that even under the condition of brittle regime machining, the propagation of microcracks was constrained at the interface between the amorphous layer and the crystalline material, and thus no damage extended into the subsurface of the crystalline material. Xu et al. [89] investigated the nanocutting mechanism of a gallium ion implantation treated surface of 6H-SiC through online observation of the cutting process using SEM. In that study, it was found that even after the layer modified by the ion implantation treatment was removed by the previous nanocutting, material removal in the ductile regime could still

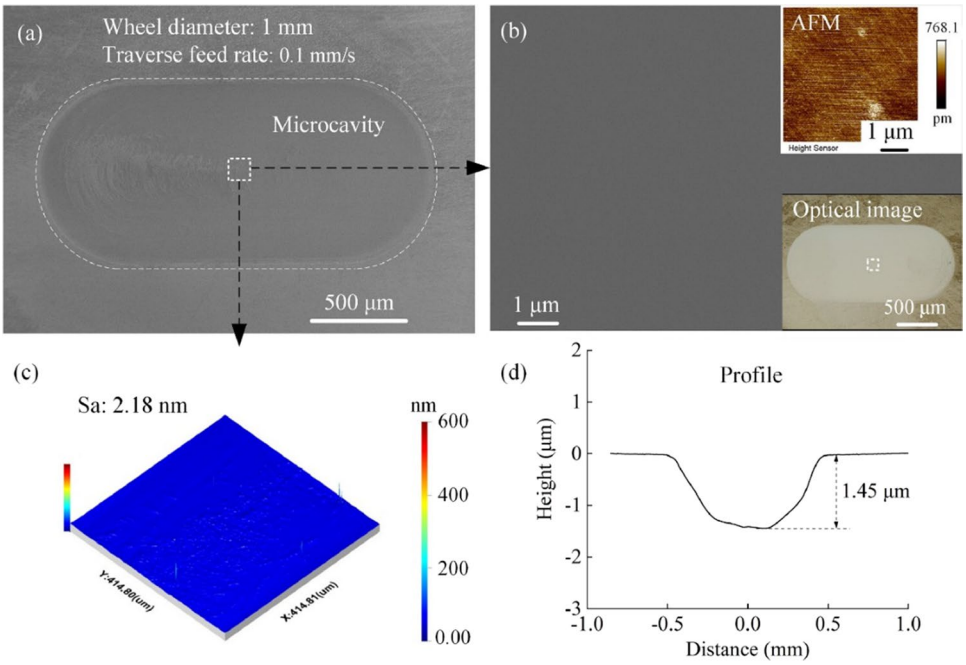

Fig. 14 Surface morphology of the micro-cavity produced by electrochemical jet-assisted mill grinding [86]. **a** Overall morphology. **b** SEM image, AFM image, and optical morphology of the cavity surface. **c** Three-dimensional morphology of the cavity surface. **d** Cross-sectional profile of the cavity

be obtained by subsequent nanocutting. This indicates that the machining efficiency of SiC can be improved by the ion implantation treatment. Liu et al. [90] conducted MD simulations of nanocutting on monocrystalline 6H-SiC to study the effect of ion implantation on the material removal mechanism. The results showed that the thickness of the machining-induced subsurface damage layer was reduced, whereas the minimum cutting thickness was increased when ion implantation was conducted prior to cutting. In addition, the cutting force, hydrostatic stress, first principal stress, and shearing stress were reduced when cutting was performed on a surface modified by ion implantation. Similar results were also reported in studies on 4H-SiC [91] and 3C-SiC [92] using MD simulations, which indicated that the machinability of monocrystalline SiC materials could be improved through surface modification by ion implantation.

3.2.2 Ion Beam Processes

Ion beam machining (IBM) is considered as one of the most advanced machining processes; in this process, a focused beam of ions is utilized to cast atoms from the work surface by elastic bombardment to fabricate desired shapes [93]. IBM has drawn attention because of its ability to fabricate microscale 3D structures with high resolution in various materials. However, very few studies have been conducted on the application of IBM for the machining of SiC. In the pioneering study by Menzel et al. [94] focused Ga^+ and Au^+ ion beams were irradiated onto 6H-SiC samples to investigate the effect of ion fluence. It was reported that with an increase in the ion fluence, sputtering rather than smoothing became more prevalent, and the volume of material removed became measurable, allowing for the fabrication of well-defined 3D structures in the material (Fig. 15). More recently, Veerapandian et al. [95] performed focused ion beam (FIB) milling of different structures to compare Si and 4H-SiC patterning. The results showed that the bottom shape of the trench being machined evolved in different ways for Si and 4H-SiC; for Si, the bottom shape changed from flat to W- and then V-shaped with the increase in ion fluence, while for SiC, it changed directly from flat to V-shaped. It was also shown that complex structures such as nano-cones were produced with a smaller aspect ratio for SiC than for Si. This was attributed to the difference in the effect of the incidence angle on the material removal rate for these materials (Fig. 16).

In the meantime, it was reported that swelling of SiC material occurs as a side effect during sputtering by the ion irradiation [96, 97]. Such swelling during ion beam processing of SiC was believed to be caused by the damage accumulation and crystalline-to-amorphous phase transformation [96]. This phenomenon could be genuinely exploited to fabricate micro/nano-scaled 3D structures on SiC [98, 99]

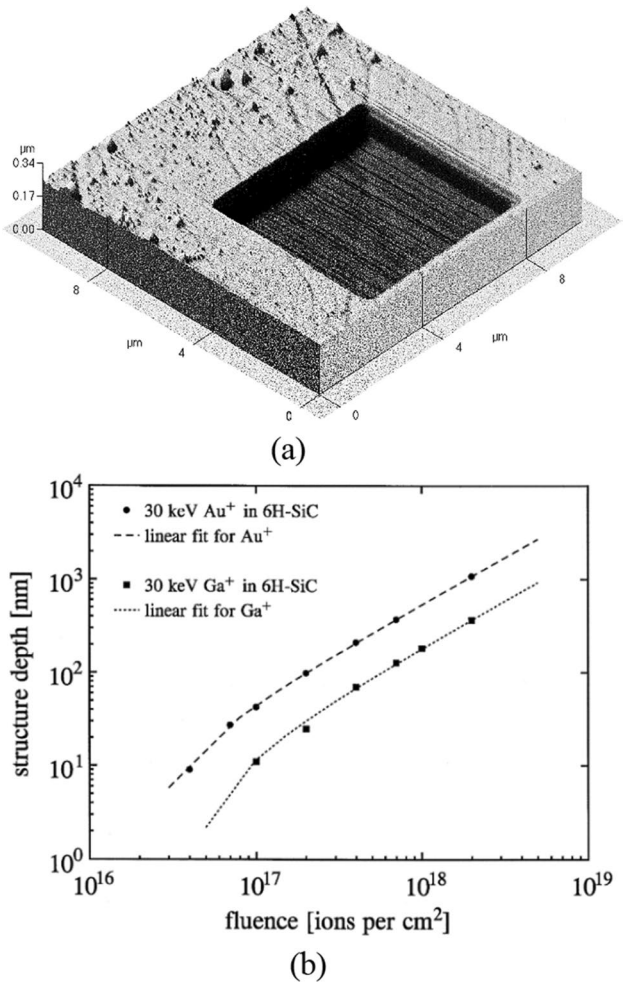

Fig. 15 Structure depth due to sputtering [94]. **a** AFM map after bombardment. **b** Structure depth as a function of the ion fluence

as can be seen in Fig. 17. In this case, the combined use of a mask could overcome the FIB's intrinsic weakness, or, slow processing speed.

3.3 Thermal Processes

3.3.1 Laser Processes

Lasers that can process materials with highly focused light energy regardless of the strength and hardness of the material have been studied for SiC processing since the early 1980s. Lasers have various wavelengths of light ranging from 157 to 10,600 nm depending on the gain medium, and the reactivity of the laser light with materials greatly depends on the wavelength. For the processing of single-crystal SiC, lasers with wavelengths in the UV range are primarily used because single-crystal SiC has a higher absorbance of UV light [100]. On the other hand, polycrystalline SiC [101] or amorphous SiC [102] can absorb visible and near-infrared

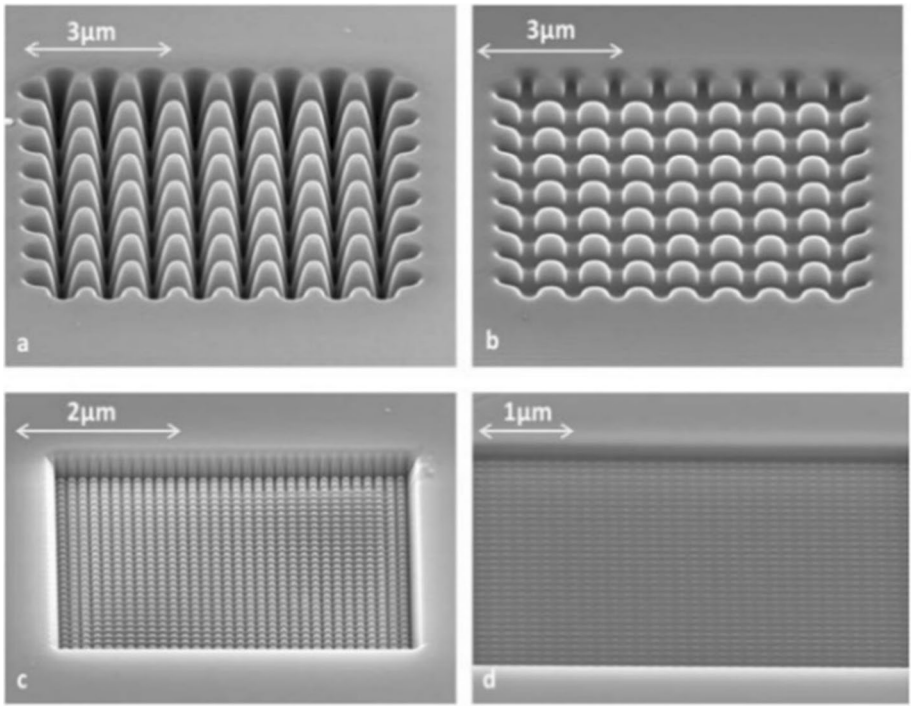

Fig. 16 Si and SiC samples with multiple horizontal and vertical lines fabricated by FIB milling using different currents, periodicities, and patterning times [95]. **a** Si 2.8 nA, 1000 nm, and 49 s. **b** SiC 2.8 nA, 1000 nm, and 99 s. **c** Si 48 pA, 150 nm, and 480 s. **d** SiC 48 pA, 150 nm, and 862 s

wavelengths; therefore, lasers with a wider range of wavelengths can be used. As described above, because the reactivity to the laser wavelength varies depending on the type of SiC, it is necessary to study the process conditions carefully to perform high-quality processing.

3.3.1.1 Long Pulse Processes For efficient processing of SiC, nanosecond pulsed short-wavelength lasers such as excimer or frequency-tripled Nd:yttrium aluminum garnet (YAG) are commonly used owing to the high absorption ratio in SiC [103]. A typical example is the manufacturing of an accelerometer based on MEMS technology by processing via a hole in a 350-μm-thick 4H-SiC wafer using a 355 nm UV laser [104]. To minimize the deterioration of the sensor performance due to the thermal effect and debris generated in the periphery, which is a disadvantage of nanosecond lasers, the same path was repeatedly irradiated with a reduced laser peak power. Consequently, a square through-hole with a width of approximately 346 μm was manufactured. The use of such a short-wavelength laser provides enhanced form accuracy for single-crystal SiC as well as amorphous SiC [105]. It has been shown that amorphous SiC can be processed at high repetition rates and low energy with a high scan speed to minimize heat damage and secondary explosions caused by debris. It was possible to process a channel with a depth of 250 μm and width of 400 μm with relatively good quality. In particular, the ArF excimer laser used in the experiment could irradiate a wide area with a uniform energy density. Therefore, a parallel process was possible using masking. Even for polycrystalline SiC, when a UV laser of 355 nm was used, it was possible to obtain a fourfold increase in light absorption compared with a 1064 nm laser [106]. Thus, a 3D spiral structure with a size of 50 μm could be fabricated, as well as a half-sphere shape.

Despite their excellent light absorption, the use of UV lasers is not efficient in terms of cost. Therefore, their application in mass production is limited [107–109]. Accordingly, various attempts have been made to process single-crystalline SiC using lasers with visible or infrared wavelengths. After irradiating the second and third harmonic generations of the Nd:YVO_4 laser on 4H-SiC, it was found that the 1064 nm laser with a large thermal effect was most effective for the surface treatment. For through-hole machining, a 355 nm laser with good light absorbance was found to be more efficient [110].

On the other hand, to increase the energy uniformity, the Gaussian beam profile can be changed to a Bessel beam profile through beam shaping, and processing can be performed in water to minimize the thermal effect. As a result, even with a 1064 nm laser, it was possible to process through-holes with a diameter of 15 μm or less in a 330-μm-thick 4H-SiC wafer [111]. In addition, various studies have been conducted using inexpensive CO_2 lasers with a long wavelength of 10.6 μm. Because the CO_2 laser has a very large thermal effect, it is possible to effectively process single-crystalline SiC even though it has high light transmittance [112]. It was possible to fabricate a through-hole with a diameter of approximately 600 μm and a thickness of 400 μm in a 4H-SiC wafer within 30 s. In the case of polycrystalline SiC, because the light absorption is relatively

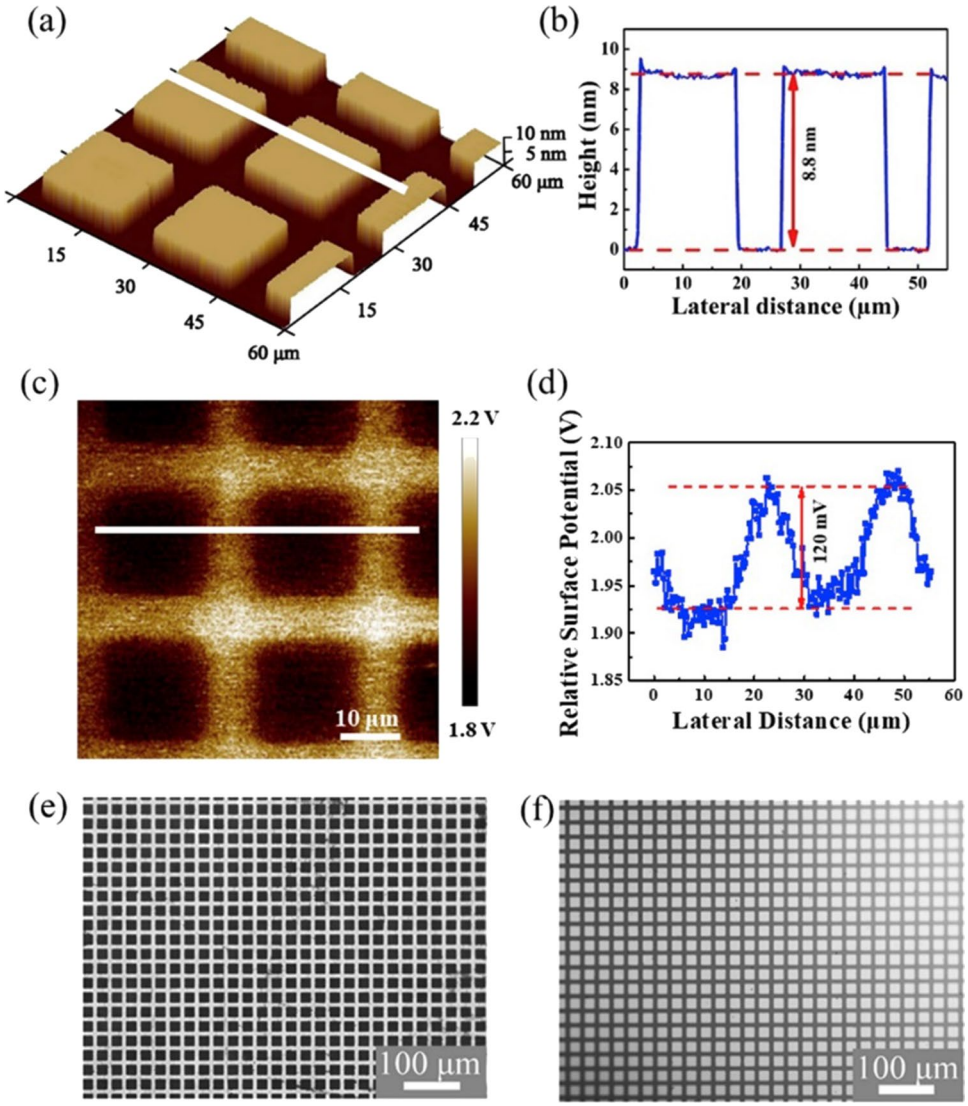

Fig. 17 Examples of micro/nanostructures fabricated on a 4H-SiC substrate using material swelling caused by ion irradiation. **a** Atomic force microscope topographical image after 20 keV Ar ion irradiation with a fluence of 7.5×10^{15} ions/cm^2 through a copper mesh mask. **b** Height profile along the white line in (**a**) showing a terrace height of ~ 8.8 nm. **c** Kelvin probe force microscope image of (**a**). **d** Relative surface potential along the white line in (**c**). **e** Optical microscope (OM) image of a copper mesh with square holes. **f** OM image of the fabricated microstructures in (**a**) using (**e**) as a mask [98]

good even in the infrared region, complex 3D structures such as microchannels can be fabricated [113]. By changing the laser scan path on a SiC sample comprising mixed α-SiC, β-SiC, and silicon, various types of microchannels can be fabricated, as shown in Fig. 18.

3.3.1.2 Ultra-short Pulse Processes When irradiating using a laser with a very high energy density, the absorption rate changes instantaneously owing to the non-linear optical effects and multi-photon absorption, eventually resulting in an excessive thermal effect. To minimize the thermal effect around the irradiated region, laser irradiation must be performed with ultra-short pulses. In theory, an ultra-short pulsed laser allows for any material, including high-band-gap dielectrics, to be machined irrespective of the laser wavelength. Therefore, machining can be effectively performed for SiC with high light transmittance [114, 115]. This was demonstrated in an experiment in which machining was conducted using both a near-infrared (NIR) laser with an ultra-short pulse and an ArF excimer laser with a nanosecond pulse [116]. Although an NIR wavelength of 1040 nm was used, when irradiated with an ultra-short pulse of 300 fs, smooth through-holes could be machined in 3C-SiC with a thickness of 400 μm. On the other hand, it was found that the ArF excimer with a nanosecond pulse improved the surface roughness owing to the melting phenomenon caused by the heat. In this context, lasers with ultra-short pulses from picoseconds to femtoseconds, which are capable of effective processing through non-linear optical absorption, have been used effectively in a variety of ways. For example, a 460-μm-diameter hole was machined by a line-scanning method using a picosecond laser [117]. Because the ultra-short pulsed laser has almost no thermal effect around the irradiated region, better results were obtained with a high-power laser, which could generate a large explosion and process rapidly, rather than a low-power

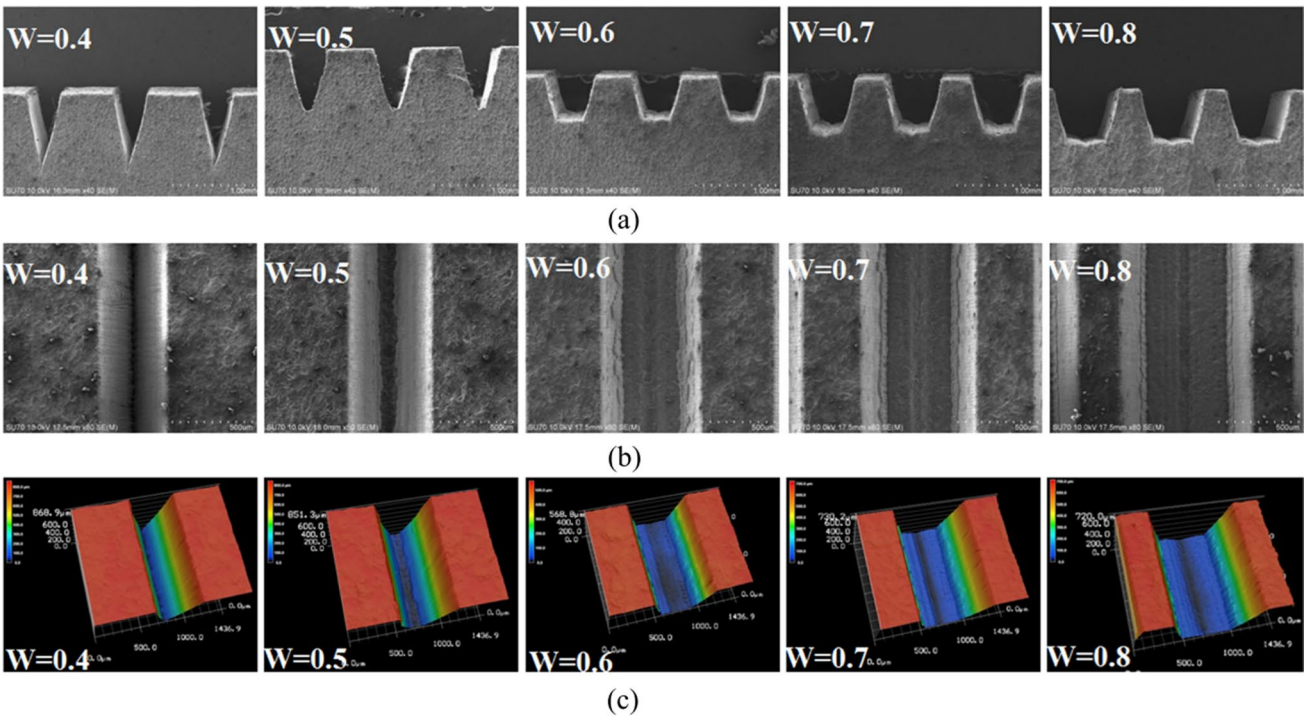

Fig. 18 Surface morphology of microchannels fabricated with different predetermined widths [113]

laser. However, at a power exceeding 10 W, pores and bubble pits due to excessive heat were also observed at the edge, suggesting that appropriate power control is required. Similar phenomena were also observed in a study using a femtosecond laser [118]. In addition, when the laser power is insufficient, a similar effect can be obtained by increasing the energy density irradiated on a local area by adjusting the feeding speed or overlapping ratio. Based on these studies, micro-3D structures can be fabricated on 3C-SiC [119] and 4H-SiC [120] with femtosecond lasers (Fig. 19). Furthermore, a femtosecond laser can be utilized to modify surface properties such as the light absorption and photocurrent rates through nano-structuring of 6H-SiC [121].

3.3.1.3 Hybrid Processes When a low-cost laser such as a nanosecond laser is used instead of ultra-short pulsed lasers, a heat-affected zone (HAZ) may be generated in the irradiated area. Thus, hybrid processes combining a water spray

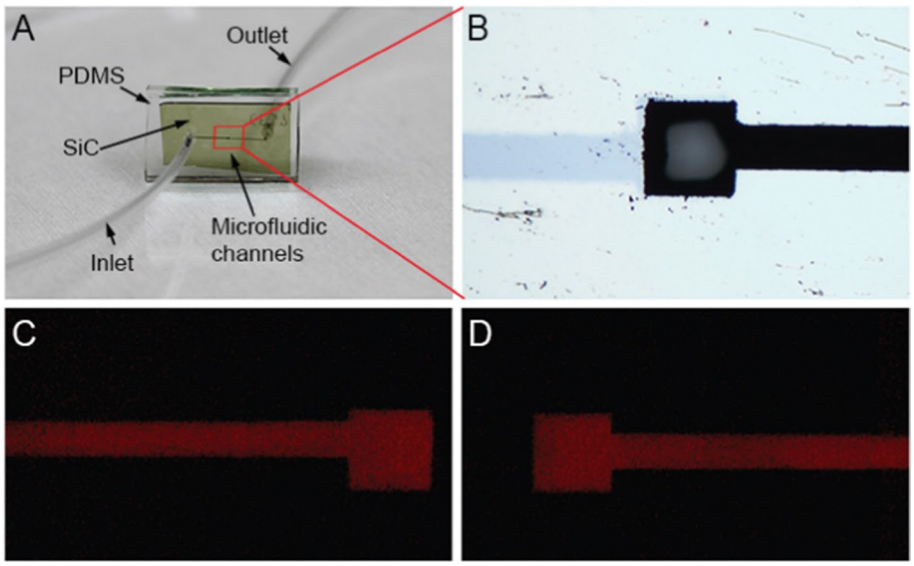

Fig. 19 Z-shaped microchannel device shown with flowing mineral oil containing red fluorescent dye [120]

with laser irradiation have been proposed to reduce the thermal reaction around the irradiated area [122]. In one study, a microchannel with a depth of 80 µm and width of 65 µm was machined on a single-crystal 4H-SiC wafer using a Yb:glass fiber laser with a pulse duration of 150 ns and wavelength of 1080 nm. To minimize the thermal effect, pressurized water (4 MPa) was sprayed on the laser processing area to form a water film for cooling. It was observed that the waterjet-assisted laser micromachining technique could significantly reduce the thermal effect compared to conventional laser processing conducted in air [123].

Alternatively, a material such as dimethylsulfoxide (DMSO, $(CH_3)_2SO$), which has an excellent cooling effect and a higher boiling temperature than water, can be used [124]. In one study, a DMSO layer with a thickness of 1–2 mm was formed above the sample surface to cool the area irradiated by a nanosecond copper vapor laser ($\lambda = 510$ nm). It was only possible to successfully fabricate a microchannel structure with a width of less than 100 µm in the presence of a DMSO liquid layer on the substrate.

3.3.2 Electrical Discharge Machining

Because SiC has very high hardness and brittleness, it is very difficult to machine SiC using conventional machining methods. Electrical discharge machining (EDM) is an electro-thermal method of material removal that can machine materials regardless of their hardness and brittleness. In addition, it does not leave burrs or cracks on the machined surface. In the EDM process, high conductivity of the workpiece is necessary. However, it has recently been shown that EDM can be used for some low-conductivity ceramics. SiC has an electrical resistivity of 13–25 mΩ cm, which is the minimum conductivity required for EDM as summarized in Fig. 20 and Table 2 [125–129].

Many studies on EDM for SiC have focused on the slicing of SiC ingots. Recently, however, some studies on sinking EDM, EDM drilling, and the EDM mechanism of SiC have been reported.

Yan et al. generated micro-craters on 4H-SiC by single discharge and experimentally investigated the atomic-scale subsurface damage during EDM of 4H-SiC as shown in Fig. 21 [129]. They characterized the subsurface damage and structural changes in the material using Raman spectroscopy and transmission electron microscopy (TEM). They

Table 2 Properties of 4H-SiC [129]

Property item	Value
Workpiece material	4H-SiC
Surface plane	(0 0 0 1)
Doping type	*n*-type
Electrical resistivity (Ω m)	$1.3–2.5 \times 10^{-4}$
Mohs hardness	~9
Thermal conductivity (W/(cm K))	370
Melting point (°C)	2730
Sublimation temperature (°C)	2830
Dielectric constant	9.76
Band gap (ev)	3.26

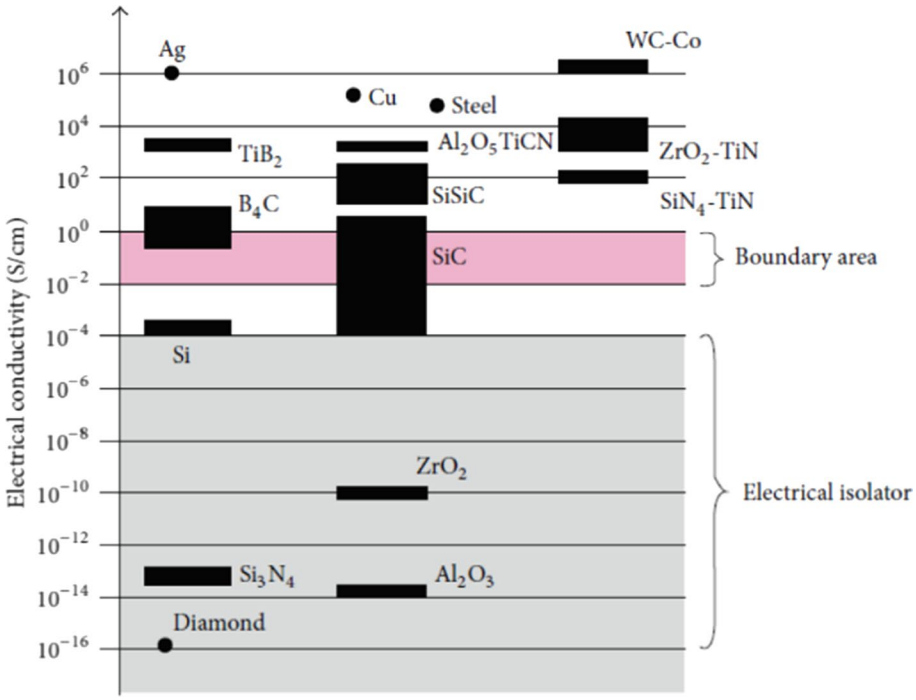

Fig. 20 Electrical conductivity of ceramic materials [125–128]

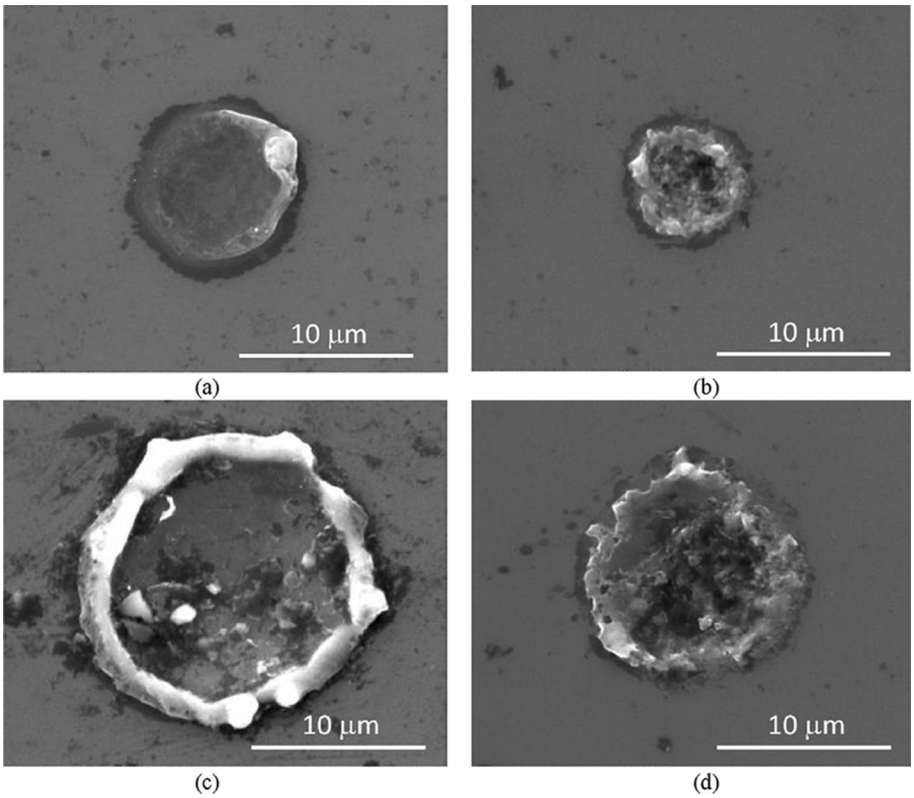

Fig. 21 SEM of micro-craters generated by single electrical discharges: **a** workpiece positive, E = 8.085 mJ; **b** workpiece negative, E = 8.085 mJ; **c** workpiece positive, E = 19.965 mJ; and **d** workpiece negative, E = 19.965 mJ [129]

also showed that SiC is decomposed into silicon and carbon during EDM and is then molten and re-solidified.

Kliuev et al. drilled blind micro-holes using deionized water and investigated the influence of EDM parameters, i.e., the pulse duration and voltage, on the material removal rate (MRR), relative tool wear, and change in the hole diameter [130].

Because SiC has become an attractive material for semiconductor power devices, an efficient slicing method for SiC ingots has also become an important issue. Although wire sawing has been widely used in ingot slicing, it is still challenging owing to the high hardness of the SiC ingots. In recent decades, many studies on wire EDM (WEDM) have been conducted for the slicing of SiC ingots and have shown that WEDM can serve as an alternative method for SiC slicing. Kato et al. showed that WEDM could be used to cut single-crystal 4H-SiC wafers and reported that WEDM produced lower surface roughness than wire sawing while achieving a maximum cutting speed of 500 μm/min [131]. Yamamoto et al. introduced a rotating WEDM slicing method for SiC ingots and improved their surface roughness. [132] Multi-wire electrodes have also been introduced to improve the efficiency of WEDM. Itokazu et al. developed a new multi-wire EDM method to slice polycrystalline SiC. They successfully demonstrated ten-wire EDM for a 100-mm-square SiC block. [133] Kimura et al. proposed a wire electrode with a tract-shaped section to provide high wire tension, which decreased the kerf width and cracks generated on the machined surface [134]. Zhao et al. proposed a copper foil electrode instead of a wire electrode for EDM slicing of 4H-SiC. Using this method, they improved the cutting speed and reduced the kerf width compared with WEDM [135, 136].

Ultrasonic vibration can be used to improve the efficiency of EDM processes. As shown in Fig. 22, Liew et al. proposed ultrasonic cavitation-assisted micro-EDM to fabricate deep micro-holes on SiC and they also added nano-fibers in the dielectric to improve the machinability and MRR and reduce the tool wear rate [137–139]. Yan et al. combined micro-EDM with micro-mill grinding to machine 4H-SiC using a PCD tool including cobalt as a binder [128]. In that hybrid machining method, SiC decomposed into C and Si in a thick recast layer created by EDM, softening the surface significantly, as shown in Fig. 23. This facilitated grinding in the ductile regime, together with the effect of the electrical discharge dressing of the PCD tool.

3.4 Additive Manufacturing

Additive manufacturing (AM), also called 3D printing, has been studied extensively because it is able to manufacture shapes with complex structures [140–142]. Compared to traditional methods such as near-net forming or

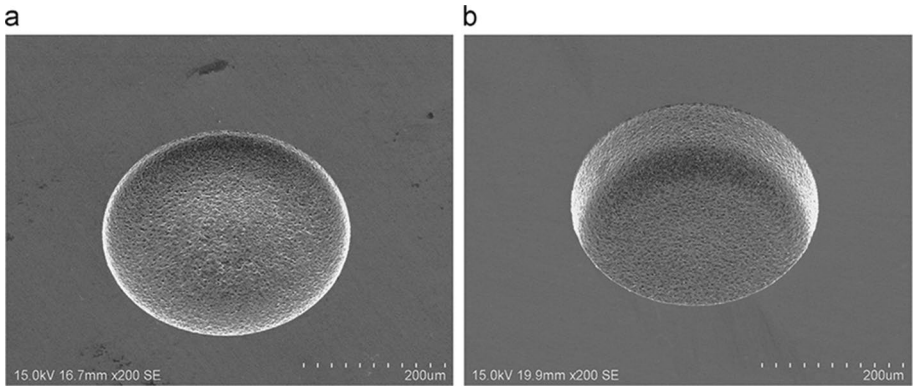

Fig. 22 SEM of micro-holes after a machining time of 2 min with ultrasonic vibration in **a** pure EDM oil and **b** carbon nanofibers mixed with EDM oil [139]

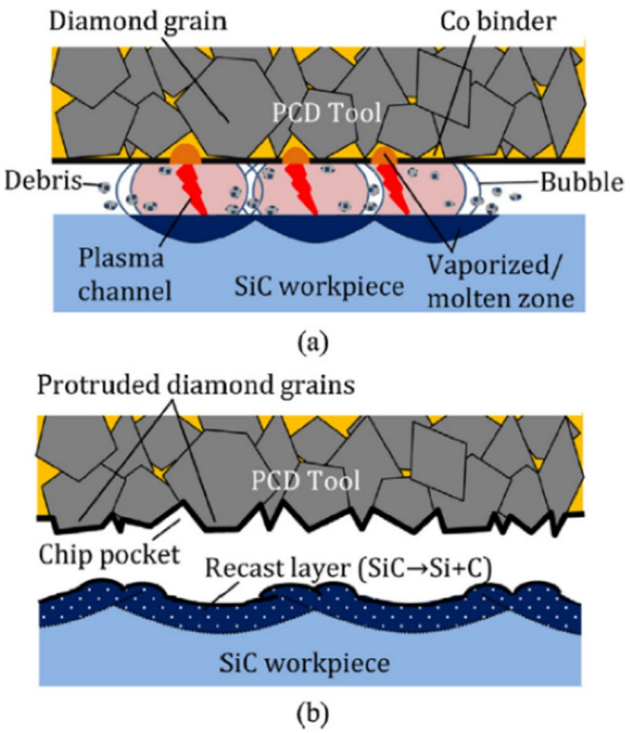

Fig. 23 Schematics of **a** material removal in EDM and **b** topographical and structural changes in PCD and SiC [128]

machining, AM is superior for small-volume customized fabrication of complex 3D structures [143]. The manufacturing of SiC ceramic structures by AM processes can generally be categorized into two types: indirect AM and direct AM. In indirect AM, a mold is made using existing AM processes, and then the SiC green body is produced from the mold [144–146]. In direct AM, in general, the SiC green body is created directly using AM processes, and thus direct AM is more capable of fabricating complex 3D structures. Therefore, in this review, we will focus on direct AM methods, which have attracted significant attention in recent years.

3.4.1 Powder Bed Fusion (PBF)

PBF processes such as selective laser sintering (SLS) and selective laser melting (SLM) mainly use lasers with high heat sources to directly attach and stack powdered materials. However, for SiC materials, it is very difficult to induce bonding between the powdered materials owing to their high melting point and low thermal conductivity. Therefore, the surface of SiC powders is generally coated with a polymer or a low-melting-point metal before AM processes are performed [147, 148]. In this case, to obtain high-purity SiC, a separate post-sintering process should be carried out. During this process, problems such as insufficient densification and defects owing to internal pores often occur. The most common method to improve defects and density is to mix a binder resin containing a large amount of carbon and Si, which has a lower melting point than SiC, and then proceed with sintering [149]. A green body mixed with a Si-SiC composite and resin matrix is formed during the AM process. Subsequently, debinding and sintering can be conducted, which increases the SiC content in the material as Si is carbonized by the carbon from the resin vaporized during the process. Consequently, SiC structures with higher densities can be obtained.

On the other hand, to obtain a highly densified Si-SiC composite green body, cold isostatic pressing (CIP) has been carried out after the PBF processes [150]. However, the greatest limitation of this reaction process is that as the densification increases, a large amount of Si that has not been converted to SiC remains inside. Therefore, to reduce unreacted Si and thus manufacture high-purity SiC parts, the precursor infiltration and pyrolysis (PIP) process was performed repeatedly (Fig. 24) [151]. This allowed for the fabrication of a part having excellent physical properties; even at a temperature of 1600 °C, the bending strength was 203.7 MPa. However, unreacted carbon and Si remain even after the repeated process is completed, which limits the fabrication of high-purity SiC structures.

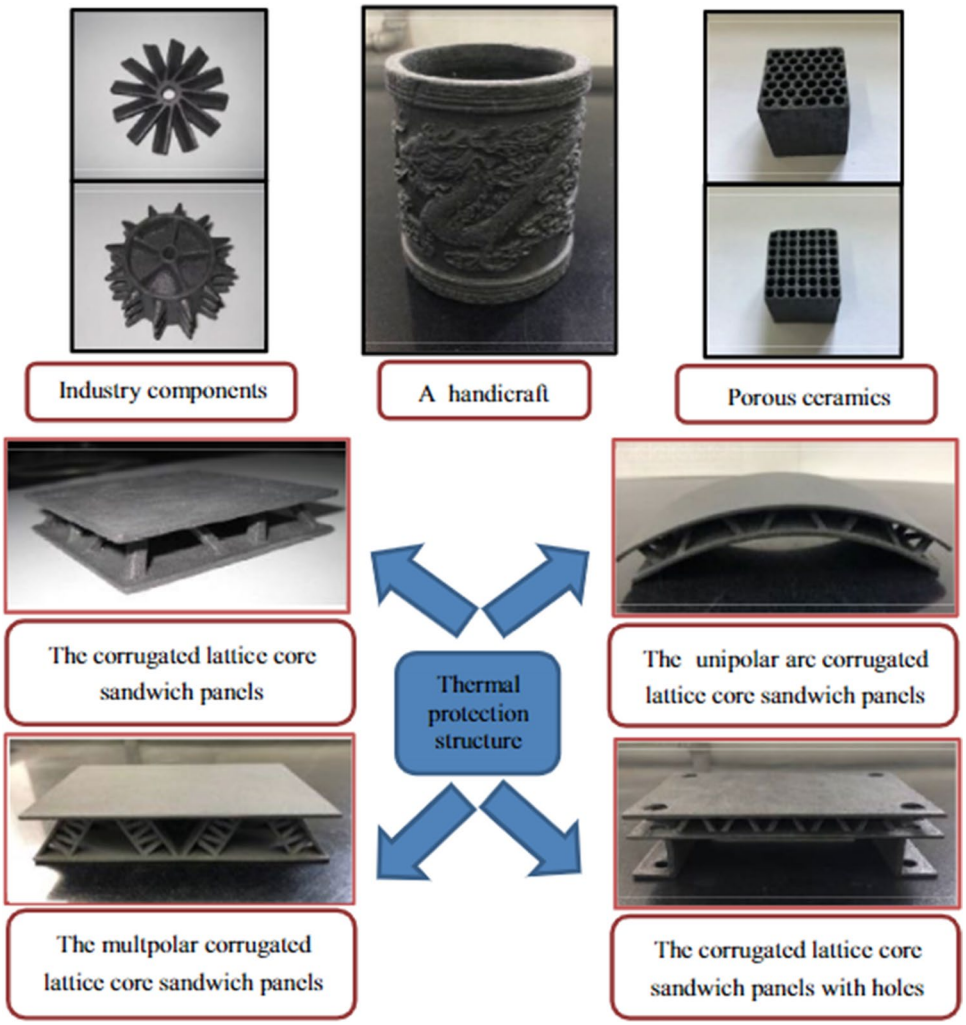

Fig. 24 SiC ceramics prepared using SLS combined with PIP [151]

3.4.2 Binder Jetting (BJ)

In BJ processes, a powdered material is spread thinly using a blade, and various adhesives are sprayed through a nozzle to produce a single layer. By repeating this bonding process, a SiC green body is formed, and the final ceramic structure is then obtained through debinding and sintering. Since ceramic AM was first introduced, many studies have investigated this process because 3D structures can be manufactured regardless of the type of powdered material. However, the strength and shape accuracy of the sintered structure are low because of the accompanying difficulties in densification [143]. Therefore, in most studies, the SiC content has been increased through the PIP process [152, 153]. Nonetheless, these processes are not suitable for manufacturing high-purity SiC structures because of their limited SiC reaction rate.

3.4.3 Material Extrusion (ME)

ME-type 3D printing processes such as fused deposition modeling (FDM), robocasting, extrusion free forming (EFF), and direct ink writing (DIW) are performed using equipment with a simple structure and are favored owing to their ability to process various materials. In most ME processes, various organic adhesive substances and dispersants are mixed with ceramic powders to form pastes, slurries, wires, etc., and the material is then extruded through a nozzle. After manufacturing a green body by continuously extruding and stacking materials, the ceramic structure is manufactured through debinding and sintering processes at high temperatures [154]. However, similar to BJ processes, the strength and shape accuracy of the structure are low; therefore, in many studies, better results could be obtained when AM processes and sintering were performed after mixing with a

material such as Al_2O_3 or Y_2O_3 rather than using only pure SiC [155, 156]. The PIP process has also been employed to maximize the SiC content and improve the density and strength [157, 158]. However, because the materials added to the mixtures to improve the structural strength and density remain in the sintered body, there is a limitation in obtaining a high purity in the final SiC structures.

3.4.4 Photo-polymerization (PP)

The PP process, often represented by stereolithography apparatus (SLA) or digital light processing (DLP), is one of the most attractive methods for the AM of SiC 3D structures because of its high precision. However, owing to the low light transmittance of SiC and the resin viscosity, which increases rapidly in proportion to the powder content, the photocurability is very low for powder composite resins with a high content [159]. Accordingly, in most studies related to the AM of SiC structures using PP, the final ceramic structure is densified through the PIP process [160–163]. In that case, a precise structure with excellent physical properties such as high strength and heat resistance can be fabricated, but there remains a limitation in building structures with high-purity SiC. In some recent studies [164, 165], after printing a composite resin including 30–40 vol% SiC powder without a precursor using DLP (Fig. 25), polymer burn-out and sintering of the green SiC ceramic were conducted at 800 °C and 1800 °C, respectively. As a result, it was possible to fabricate high-purity 6H-SiC structures; however, the relative density was 85% or less owing to the limitation in the powder content. Consequently, the flexural strength was measured as 78.6 MPa, which is approximately 20% that of bulk SiC. To improve the mechanical properties, the PIP process was performed eight times, resulting in a flexural strength of 165.2 MPa, which is twice as high as that without the PIP process. Although the SiC powder content could be increased compared to other AM processes, the degree of densification remains low, and thus there is a limit to the production of high-purity SiC structures with sufficient strength for practical use.

4 Summary

This paper presents a review of the machining processes for SiC. First, we introduce SiC materials and their applications. Then, we summarize four major fabrication methods for microscale 3D structures of SiC: etching, mechanical processes, thermal processes, and AM. The structures of SiC are divided into amorphous, polycrystalline, and single-crystalline structures, which depend on the manufacturing processes. The crystal structure causes differences in the mechanical, optical, and electrical properties of SiC. 4H-SiC is preferred for power electronic device applications because of its high carrier mobility. 3C-SiC is more commonly used for MEMS-based sensors owing to its low wafer cost. Sintered SiC is widely used in mechanical devices and parts owing to its high hardness.

SiC has high mechanical, thermal, and chemical resistance. Therefore, fabricating micro-features on SiC is

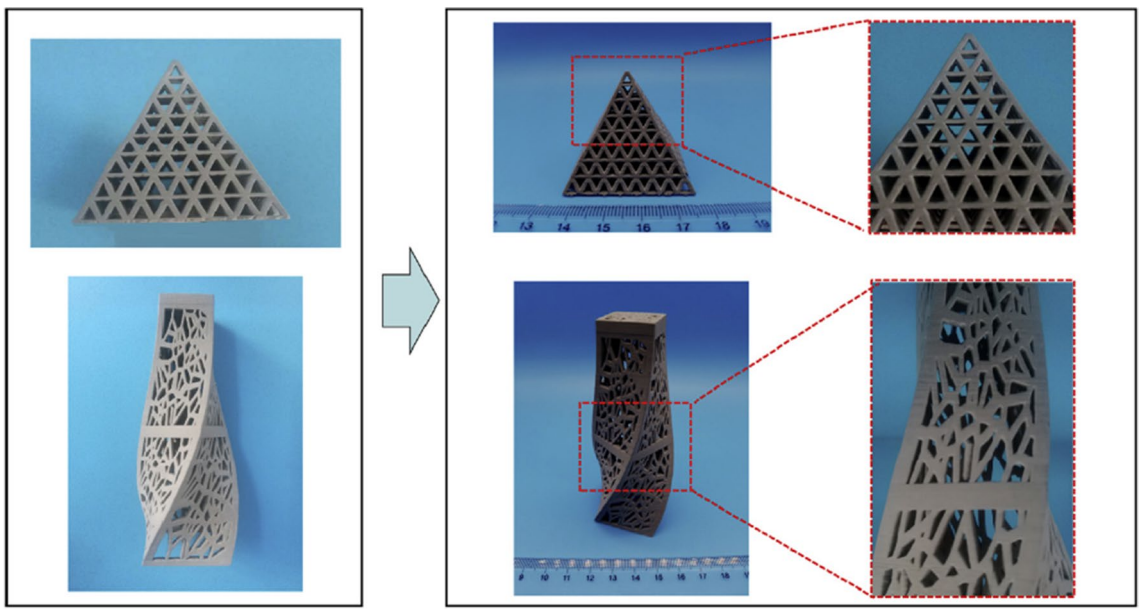

Fig. 25 Stereolithography of SiC ceramic architectures with pyramid and hollowed basket structures: green SiC structures and final SiC structures after PIP [165]

expensive and time-consuming. Because SiC has a high resistance to all known aqueous etching solutions, etching of SiC is very challenging. Although hybrid methods such as electrochemical etching and photoelectrochemical etching have been reported, one of the most popular methods is plasma-based dry etching, which is considered the only practical method in the SiC etching industry. ICP etching, a plasma-based dry-etching method, has been widely used in the fabrication of SiC devices. It has several advantages, such as simple operation, easy automatic control, and availability for large-area substrate etching. Owing to the high brittleness of SiC, mechanical methods are used only for a limited number of applications. Single and polycrystalline diamond micro-tools are used to generate 3D microstructures of SiC. To overcome the low machinability of SiC, hybrid mechanical methods combining laser, ultrasonic vibration, and electrochemical processes have been reported. Laser processes and EDM are among the available thermal methods. Lasers of various wavelengths, such as Nd:YAG, excimer, and CO_2 lasers, can be used, and the machinability depends on the laser transmittance or absorbance of SiC materials. To prevent thermal damage and obtain a better surface quality, an ultra-short pulsed laser is used. Although SiC has low electrical conductivity, it can be machined using EDM. Many studies have focused on slicing SiC ingots for SiC wafer production. Because conventional wire sawing suffers from the high hardness of SiC, wire EDM can be used as an alternative method. Among additive methods, PP is one of the most attractive methods for producing 3D structures. However, because the printable material is a SiC composite rather than high-purity SiC, it does not provide sufficient strength for practical use.

This paper reviews the processes applicable for microscale 3D structuring of silicon carbide. Although SiC is a very attractive material for many applications, the fabrication of microscale structures on SiC remains challenging. The development and improvement of fabrication methods for SiC are required and are promising research topics.

Acknowledgements This work was supported by the Technology Innovation Program (20010984) funded By the Ministry of Trade, Industry & Energy (MOTIE, Korea)

References

1. Foti, G. (2001). Silicon carbide: From amorphous to crystalline material. *Applied Surface Science, 184*(1–4), 20–26.
2. Yang, C. Y., Rahman, M. M., & Harris, G. L. (1992). *Amorphous and crystalline silicon carbide IV* Springer proceedings in physics (Vol. 71). Springer.
3. Oliveros, A., Guiseppi-Elie, A., & Saddow, S. E. (2013). Silicon carbide: A versatile material for biosensor applications. *Biomedical Microdevices, 15*(2), 353–368.
4. Munro, R. G. (1997). Material properties of a sintered α-SiC. *Journal of Physical and Chemical Reference Data, 26*(5), 1195–1203.
5. Powell, A. R., & Rowland, L. B. (2002). SiC materials—Progress, status, and potential roadblocks. *Proceedings of the IEEE, 90*(6), 942–955.
6. Gerhardt, R. (2011). *Properties and applications of silicon carbide*. Intech.
7. Elasser, A., & Chow, T. P. (2002). Silicon carbide benefits and advantages for power electronics circuits and systems. *Proceedings of the IEEE, 90*(6), 969–986.
8. Wright, N. G., & Horsfall, A. B. (2007). SiC sensors: A review. *Journal of Physics D: Applied Physics, 40*(20), 6345–6354.
9. Xu, M., Girish, Y. R., Rakesh, K. P., Wu, P., Manukumar, H. M., Byrappa, S. M., & Byrappa, K. (2021). Recent advances and challenges in silicon carbide (SiC) ceramic nanoarchitectures and their applications. *Materials Today Communications, 28*, 102533.
10. Zhuang, D., & Edgar, J. H. (2005). Wet etching of GaN, AlN, and SiC: A review. *Materials Science and Engineering R: Reports, 48*(1), 1–46.
11. Abderrazak, H., & Hadj Hmi, E. S. B. (2011). Silicon carbide: Synthesis and Properties. In *Properties and applications of silicon carbide*.
12. Li, J., & Zhang, G.-Q. (2019). Light-emitting diodes. *Materials, Processes, Devices and Applications, 4*, 600–600.
13. Brezeanu, G., Badila, M., Draghici, F., Pascu, R., Pristavu, G., Craciunoiu, F., & Rusu, I. (2015). High temperature sensors based on silicon carbide (SiC) devices. In *Proceedings of the international semiconductor conference, CAS, 2015* (pp. 3–10).
14. Ji, S., Zhang, Z., & Wang, F. (2020). Overview of high voltage sic power semiconductor devices: Development and application. *CES Transactions on Electrical Machines and Systems, 1*(3), 254–264.
15. Watari, K., & Shinde, S. L. (2001). *High thermal conductivity materials* (Vol. 26, pp. 440–441). Springer.
16. Rosenbloom, A. J., Sipe, D. M., Shishkin, Y., Ke, Y., Devaty, R. P., & Choyke, W. J. (2004). Nanoporous SiC: A candidate semi-permeable material for biomedical applications. *Biomedical Microdevices, 6*(4), 261–267.
17. Beke, D., Szekrényes, Z., Pálfi, D., Róna, G., Balogh, I., Maák, P. A., Katona, G., Czigány, Z., Kamarás, K., Rózsa, B., Buday, L., Vértessy, B., & Gali, A. (2013). Silicon carbide quantum dots for bioimaging. *Journal of Materials Research, 28*(2), 205–209.
18. Li, X., Wang, X., Bondokov, R., Morris, J., An, Y. H., & Sudarshan, S. (2005). Micro/nanoscale mechanical and tribological characterization of SiC for orthopedic applications. *Journal of Biomedical Materials Research Part B: Applied Biomaterials, 72B*(2), 353–361.
19. Yakimova, R., Petoral, R. M., Yazdi, G. R., Vahlberg, C., Lloyd Spetz, A., & Uvdal, K. (2007). Surface functionalization and biomedical applications based on SiC. *Journal of Physics D: Applied Physics, 40*(20), 6435–6442.
20. Phan, H. P., Dao, D. V., Nakamura, K., Dimitrijev, S., & Nguyen, N.-T. (2015). The piezoresistive effect of SiC for MEMS sensors at high temperatures: A review. *Journal of Microelectromechanical Systems, 24*(6), 1663–1677.
21. Pham, T. A., Qamar, A., Dinh, T., Masud, M. K., Rais-Zadeh, M., Senesky, D. G., Yamauchi, Y., Nguyen, N. T., & Phan, H. P. (2020). Nanoarchitectonics for wide bandgap semiconductor nanowires: Toward the next generation of nanoelectromechanical systems for environmental monitoring. *Advanced Science, 7*(21), 1–30.
22. Lin, X., Lin, S., Xu, Y., Hakro, A. A., Hasan, T., Zhang, B., Yu, B., Luo, J., Li, E., & Chen, H. (2013). Ab initio study

of electronic and optical behavior of two-dimensional silicon carbide. *Journal of Materials Chemistry C, 1*(11), 2131.
23. Kudimi, J. M. R., Mohd-Yasin, F., & Dimitrijev, S. (2012). Sic-based piezoelectric energy harvester for extreme environment. *Procedia Engineering, 47*, 1165–1172.
24. Katsuno, M., Ohtani, N., Takahashi, J., Yashiro, H., & Kanaya, M. (1999). Mechanism of molten KOH etching of SiC single crystals: Comparative study with thermal oxidation. *Japanese Journal of Applied Physics, Part 1: Regular Papers and Short Notes and Review Papers, 38*(8 B), 4661–4665.
25. Harris, J. M., Gatos, H. C., & Witt, A. F. (1969). Identification of the (0001) and the (0001) surfaces of silicon carbide. *Journal of the Electrochemical Society, 116*(5), 672–672.
26. Tan, J. H., Chen, Z. Z., Lu, W. Y., Cheng, Y., He, H., Liu, Y. H., Sun, Y. J., & Zhao, G. J. (2014). Fabrication of uniform 4H-SiC mesopores by pulsed electrochemical etching. *Nanoscale Research Letters, 9*(1), 3–7.
27. Zhan, S., Dong, B., Wang, H., & Zhao, Y. (2021). A novel approach for bulk micromachining of 4H-SiC by tool-based electrolytic plasma etching in HF-free aqueous solution. *Journal of the European Ceramic Society, 41*(10), 5075–5087.
28. Chen, Y., Zhang, C., Li, L., Zhou, S., Chen, X., Gao, J., Zhao, N., & Wong, C. P. (2019). Hybrid anodic and metal-assisted chemical etching method enabling fabrication of silicon carbide nanowires. *Small (Weinheim an der Bergstrasse, Germany), 15*, 1803898.
29. Shishkin, Y., Choyke, W. J., & Devaty, R. P. (2004). Photoelectrochemical etching of n-type 4H silicon carbide. *Journal of Applied Physics, 96*(4), 2311–2322.
30. Zhao, F., Islam, M. M., & Huang, C. F. (2011). Photoelectrochemical etching to fabricate single-crystal SiC MEMS for harsh environments. *Materials Letters, 65*(3), 409–412.
31. Jiang, L., Plank, N. O., Blauw, M. A., Cheung, R., & van der Drift, E. W. (2004). Dry etching of SiC in inductively coupled Cl2/Ar plasma. *Journal of Physics D: Applied Physics, 37*(13), 1809–1814.
32. Zhuang, S., Tang, J., Gu, Z., Che, D., Hu, D., Chen, L., & Xu, K. (2019). Microscale pattern etch of 4H–SiC by inductively coupled plasma. *Journal of Materials Science: Materials in Electronics, 30*, 18788–18793.
33. Choi, J. H., Latu-Romain, L., Bano, E., Dhalluin, F., Chevolleau, T., & Baron, T. (2012). Fabrication of SiC nanopillars by inductively coupled SF_6/O_2 plasma etching. *Journal of Physics D: Applied Physics, 45*(23), 235204.
34. Dowling, K. M., Ransom, E. H., & Senesky, D. G. (2017). Profile evolution of high aspect ratio silicon carbide trenches by inductive coupled plasma etching. *Journal of Microelectromechanical Systems, 26*(1), 135–142.
35. Luna, L. E., et al. (2017). Dry Etching of High Aspect Ratio 4H-SiC Microstructures. *ECS Journal of Solid State Science and Technology, 6*(4), P207–P210.
36. Osipov, A. A., Iankevich, G. A., Osipov, A. A., Speshilova, A. B., Karakchieva, A. A., Endiiarova, E. V., Levina, S. N., Karakchiev, S. V., & Alexandrov, S. E. (2021). Silicon carbide dry etching technique for pressure sensors design. *Journal of Manufacturing Processes, 2022*(73), 316–325.
37. Osipov, A. A., Iankevich, G. A., Speshilova, A. B., Osipov, A. A., Endiiarova, E. V., Berezenko, V. I., Tyurikova, I. A., Tyurikov, K. S., & Alexandrov, S. E. (2020). High-temperature etching of SiC in SF_6/O_2 inductively coupled plasma. *Scientific Reports, 10*(1), 19977.
38. Ru, H., Yin-Tang, Y., & Xiao-Ya, F. (2009). Microtrenching geometry of 6H-SiC plasma etching. *Vacuum, 84*, 400–404.
39. Fukunaga, K., Suda, J., & Kimoto, T. (2006). Anisotropic etching of single crystalline SiC using molten KOH for SiC bulk micromachining. *Micromachining and Microfabrication Process Technology XI, 6109*, 61090G-61090G.
40. Henkel, T., Ferro, G., Nishizawa, S. I., Pressler, H., Tanaka, Y., Tanoue, H., & Kobayashi, N. (2000). Structural characterization of silicon carbide etched by using a combination of ion implantation and wet chemical etching. *Materials Science Forum, 338–342*, 481–484.
41. Alok, D., & Baliga, B. J. (1995). A novel method for etching trenches in silicon carbide. *Journal of Electronic Materials, 24*(4), 311–314.
42. van Dorp, D. H., Sattler, J. J. H. B., den Otter, J. H., & Kelly, J. J. (2009). Electrochemistry of anodic etching of 4H and 6H–SiC in fluoride solution of pH 3. *Electrochimica Acta, 54*(26), 6269–6275.
43. Chen, C., Chen, S., Shang, M., Gao, F., Yang, Z., Liu, Q., He, Z., & Yang, W. (2016). Fabrication of highly oriented 4H-SiC gourd-shaped nanowire arrays and their field emission properties. *Journal of Materials Chemistry C, 4*(23), 5195–5201.
44. Leitgeb, M., Zellner, C., Schneider, M., Schwab, S., Hutter, H., & Schmid, U. (2017). Metal assisted photochemical etching of 4H silicon carbide. *Journal of Physics D: Applied Physics, 50*(43), 435.
45. Racka-Szmidt, K., Stonio, B., Żelazko, J., Filipiak, M., & Sochacki, M. (2022). A review: Inductively coupled plasma reactive ion etching of silicon carbide. *Materials, 15*(1), 123.
46. Sung, H. K., Qiang, T., Yao, Z., Li, Y., Wu, Q., Lee, H. K., Park, B. D., Lim, W. S., Park, K. H., & Wang, C. (2017). Vertical and bevel-structured SiC etching techniques incorporating different gas mixture plasmas for various microelectronic applications. *Scientific Reports, 7*(1), 1–9.
47. Sano, Y., Aida, K., Nishikawa, H., Yamamura, K., Matsuyama, S., & Yamauchi, K. (2012). Back-side thinning of silicon carbide wafer by plasma etching using atmospheric-pressure plasma. *Key Engineering Materials, 516*, 108–112.
48. Habuka, H., Oda, S., Fukai, Y., Fukae, K., Takeuchi, T., & Aihara, M. (2005). Silicon carbide etching using chlorine trifluoride gas. *Japanese Journal of Applied Physics, Part 1: Regular Papers and Short Notes and Review Papers, 44*(3), 1376–1381.
49. Habuka, H., Oda, S., Fukai, Y., Fukae, K., Takeuchi, T., & Aihara, M. (2006). Etch rate and surface morphology of polycrystalline β-silicon carbide using chlorine trifluoride gas. *Thin Solid Films, 514*(1–2), 193–197.
50. Habuka, H., Tanaka, K., Katsumi, Y., Takechi, N., Fukae, K., & Kato, T. (2009). Temperature-dependent behavior of 4H-silicon carbide surface morphology etched using chlorine trifluoride gas. *Journal of The Electrochemical Society, 156*(12), H971–H971.
51. Bifano, T. G., Dow, T. A., & Scattergood, R. O. (1991). Ductile-regime grinding: A new technology for machining brittle materials. *Journal of Engineering for Industry, 113*(2), 6–6.
52. Patten, J., Gao, W., & Yasuto, K. (2005). Ductile regime nanomachining of single-crystal silicon carbide. *Journal of Manufacturing Science and Engineering, 127*(3), 522–532.
53. Patten, J. A., & Jacob, J. (2008). Comparison between numerical simulations and experiments for single-point diamond turning of single-crystal silicon carbide. *Journal of Manufacturing Processes, 10*(1), 28–33.
54. Xiao, G., To, S., & Zhang, G. (2015). The mechanism of ductile deformation in ductile regime machining of 6H SiC. *Computational Materials Science, 98*, 178–188.
55. Zhu, D., Yan, S., & Li, B. (2014). Single-grit modeling and simulation of crack initiation and propagation in SiC grinding using maximum undeformed chip thickness. *Computational Materials Science, 92*, 13–21.

56. Blackley, W. S., & Scattergood, R. O. (1991). Ductile-regime machining model for diamond turning of brittle materials. *Precision Engineering, 13*(2), 95–103.
57. Goel, S., Luo, X., Comley, P., Reuben, R. L., & Cox, A. (2013). Brittle–ductile transition during diamond turning of single crystal silicon carbide. *International Journal of Machine Tools and Manufacture, 65*, 15–21.
58. Bifano, T., Yi, Y., & Kahl, K. (1994). Fixed abrasive grinding of CVD SiC mirrors. *Precision Engineering, 16*(2), 109–116.
59. Ling Yin, E. Y. J., Vancoille, L. C. L., Huang, H., Ramesh, K., & Liu, X. D. (2004). High-quality grinding of polycrystalline silicon carbide spherical surfaces. *Wear, 256*(1–2), 197–207.
60. Beaucamp, A., Simon, P., Charlton, P., King, C., Matsubara, A., & Wegener, K. (2017). Brittle–ductile transition in shape adaptive grinding (SAG) of SiC aspheric optics. *International Journal of Machine Tools and Manufacture, 115*, 29–37.
61. Namba, Y., Kobayashi, H., Suzuki, H., Yamashita, K., & Taniguchi, N. (1999). Ultraprecision surface grinding of chemical vapor deposited silicon carbide for X-ray mirrors using resinoid-bonded diamond wheels. *CIRP Annals, 48*(1), 277–280.
62. Zhong, Z., & Nakagawa, T. (1996). Grinding of aspherical SiC mirrors. *Journal of Materials Processing Technology, 56*(1), 37–44.
63. Beaucamp, A., Namba, Y., Combrinck, H., Charlton, P., & Freeman, R. (2014). Shape adaptive grinding of CVD silicon carbide. *CIRP Annals, 63*(1), 317–320.
64. Horvath, N., Honeycutt, A., & Davies, M. A. (2020). Grinding of additively manufactured silicon carbide surfaces for optical applications. *CIRP Annals, 69*(1), 509–512.
65. Wang, S., Zhao, Q., Guo, B., & Pan, Y. (2020). Ultra-precision raster grinding of monocrystalline silicon biconical free-form optics using arc-shaped diamond grinding wheels. *Journal of Manufacturing Processes, 58*, 1064–1074.
66. Xie, J., Li, Q., Sun, J. X., & Li, Y. H. (2015). Study on ductile-mode mirror grinding of SiC ceramic freeform surface using an elliptical torus-shaped diamond wheel. *Journal of Materials Processing Technology, 222*, 422–433.
67. Takesue, S., Katahira, K., & Komotori, J. (2014). A study on PCD tool surface reconditioning technique for SiC micromachining. *Procedia CIRP, 14*, 355–359.
68. Katahira, K., Takesue, S., Komotori, J., & Yamazaki, K. (2014). Micromilling characteristics and electrochemically assisted reconditioning of polycrystalline diamond tool surfaces for ultra-precision machining of high-purity SiC. *CIRP Annals, 63*(1), 329–332.
69. Suzuki, H., Okada, M., Asai, W., Sumiya, H., Harano, K., Yamagata, Y., & Miura, K. (2017). Micro milling tool made of nano-polycrystalline diamond for precision cutting of SiC. *CIRP Annals, 66*(1), 93–96.
70. Cvetković, S., Morsbach, C., & Rissing, L. (2011). Ultra-precision dicing and wire sawing of silicon carbide (SiC). *Microelectronic Engineering, 88*(8), 2500–2504.
71. Yang, Z., Zhu, L., Zhang, G., Ni, C., & Lin, B. (2020). Review of ultrasonic vibration-assisted machining in advanced materials. *International Journal of Machine Tools and Manufacture, 156*, 103594–103594.
72. Cao, J., Wu, Y., Lu, D., Fujimoto, M., & Nomura, M. (2014). Material removal behavior in ultrasonic-assisted scratching of SiC ceramics with a single diamond tool. *International Journal of Machine Tools and Manufacture, 79*, 49–61.
73. Yan, L., Zhang, X., Li, H., & Zhang, Q. (2022). Machinability improvement in three-dimensional (3D) ultrasonic vibration assisted diamond wire sawing of SiC. *Ceramics International, 48*, 8051–8068.
74. Zhao, L., Zhang, J., Zhang, J., & Hartmaier, A. (2021). Atomistic investigation of machinability of monocrystalline 3C–SiC in elliptical vibration-assisted diamond cutting. *Ceramics International, 47*(2), 2358–2366.
75. Guo, B., Zhao, Q. L., & Jackson, M. J. (2012). Ultrasonic vibration-assisted grinding of micro-structured surfaces on silicon carbide ceramic materials. *Proceedings of the Institution of Mechanical Engineers, Part B: Journal of Engineering Manufacture, 226*(3), 553–559.
76. Jiang, Y., Li, J., Zhou, Z., Jiang, X., & Zhang, D. (2016). Fabrication of all-sic fiber-optic pressure sensors for high-temperature applications. *Sensors, 16*(10), 1660.
77. Li, J., Geng, D., Zhang, D., Qin, W., & Jiang, Y. (2018). Ultrasonic vibration mill-grinding of single-crystal silicon carbide for pressure sensor diaphragms. *Ceramics International, 44*(3), 3107–3112.
78. Banik, S. R., Kalita, N., Gajrani, K. K., Kumar, R., & Sankar, M. R. (2018). Recent trends in laser assisted machining of ceramic materials. *Materials Today: Proceedings, 5*(9), 18459–18467.
79. Bharat, N., & Bose, P. S. C. (2021). An overview on machinability of hard to cut materials using laser assisted machining. *Materials Today: Proceedings, 43*, 665–672.
80. Patten, J. A. (2009). Pressure and temperature effects in micro-laser assisted machining (μ-LAM) of silicon carbide. *Transactions of NAMRI/SME, 37*, 75–80.
81. Ravindra, D., Virkar, S., & Patten, J. (2011). Ductile mode micro laser assisted machining of silicon carbide (SiC), In R. Gerhardt (Ed.), InTech. (pp. 506–535).
82. Shayan, A. R., Poyraz, H. B., Ravindra, D., Ghantasala, M., & Patten, J. A. (2009). Force analysis, mechanical energy and laser heating evaluation of scratch tests on silicon carbide (4H-SIC) in micro-laser assisted machining (μ-LAM) process. In *Proceedings of the ASME 2009 international manufacturing science and engineering conference*. West Lafayette, Indiana.
83. Virkar, S. R. & Patten, J. A. (2009). Numerical simulations and analysis of the thermal effects on silicon carbide during ductile mode micro-laser assisted machining. In *Proceedings of the ASME 2009 international manufacturing science and engineering conference*. West Lafatyette, Indiana, USA.
84. Meng, B., Yuan, D., Zheng, J., & Xu, S. (2019). Molecular dynamics study on femtosecond laser aided machining of monocrystalline silicon carbide. *Materials Science in Semiconductor Processing, 101*, 1–9.
85. Katahira, K., Ohmori, H., Takesue, S., Komotori, J., & Yamazaki, K. (2015). Effect of atmospheric-pressure plasma jet on polycrystalline diamond micro-milling of silicon carbide. *CIRP Annals, 64*(1), 129–132.
86. Chen, Z., Zhan, S., & Zhao, Y. (2021). Electrochemical jet-assisted precision grinding of single-crystal SiC using soft abrasive wheel. *International Journal of Mechanical Sciences, 195*, 106239–106239.
87. Fang, F. Z., Chen, Y. H., Zhang, X. D., Hu, X. T., & Zhang, G. X. (2011). Nanometric cutting of single crystal silicon surfaces modified by ion implantation. *CIRP Annals - Manufacturing Technology, 60*(1), 527–530.
88. Tanaka, H., & Shimada, S. (2013). Damage-free machining of monocrystalline silicon carbide. *CIRP Annals - Manufacturing Technology, 62*(1), 55–58.
89. Xu, Z., Liu, L., He, Z., Tian, D., Hartmaier, A., Zhang, J., Luo, X., Rommel, M., Nordlund, K., Zhang, G., & Fang, F. (2020). Nanocutting mechanism of 6H-SiC investigated by scanning electron microscope online observation and stress-assisted and ion implant-assisted approaches. *International Journal of Advanced Manufacturing Technology, 106*(9–10), 3869–3880.
90. Liu, B., Xu, Z., Wang, Y., Gao, X., & Kong, R. (2020). Effect of ion implantation on material removal mechanism of 6H-SiC in nano-cutting: A molecular dynamics study. *Computational Materials Science, 174*, 109476.

91. Fan, Y., Xu, Z., Song, Y., Dong, B., Xue, Z., Liu, B., Liu, L., & Tian, D. (2021). Nano material removal mechanism of 4H-SiC in ion implantation-assisted machining. *Computational Materials Science, 200*, 110837.
92. Dai, H., Hu, Y., Wu, W., Yue, H., Meng, X., Li, P., & Duan, H. (2021). Molecular dynamics simulation of ultra-precision machining 3C-SiC assisted by ion implantation. *Journal of Manufacturing Processes, 69*, 398–411.
93. Bhattacharyya, B., & Doloi, B. (2020). *Machining processes utilizing mechanical energy* (pp. 21–160). Academic Press.
94. Menzel, R., Bachmann, T., Machalett, F., Wesch, W., Lang, U., Wendt, M., Musil, C., & Mühle, R. (1998). Surface smoothing and patterning of SiC by focused ion beams. *Applied Surface Science, 136*(1), 1–7.
95. Veerapandian, S. K., Beuer, S., Rumler, M., Stumpf, F., Thomas, K., Pillatsch, L., Michler, J., Frey, L., & Rommel, M. (2015). Comparison of silicon and 4H silicon carbide patterning using focused ion beams. *Nuclear Instruments and Methods in Physics Research, Section B: Beam Interactions with Materials and Atoms, 365*, 44–49.
96. McHargue, C. J., & Williams, J. M. (1993). Ion implantation effects in silicon carbide. *Nuclear Instruments and Methods in Physics Research Section B: Beam Interactions with Materials and Atoms, 80–81*, 889–894.
97. Bischoff, L., Teichert, J., & Heera, V. (2001). Focused ion beam sputtering investigations on SiC. *Applied Surface Science, 184*(1), 372–376.
98. Zhou, Y., Li, S., Wang, Y., Huang, Q., Zhang, W., Yao, Y., Hao, J., Sun, Y., Tang, M., Li, B., & Zhang, Y. (2019). One-step ion beam irradiation manufacture of 3D micro/nanopatterned structures in SiC with tunable work functions. *Carbon, 148*, 387–393.
99. Momota, S., Sato, N., & Honda, K. (2019). Fabrication of multi-step swelling structures on 6H–SiC by using highly-charged Ar beams. *Vacuum, 170*, 108963.
100. Pecholt, B., Gupta, S., & Molian, P. (2011). Review of laser microscale processing of silicon carbide. *Journal of Laser Applications, 23*(1), 012008–012008.
101. Sciti, D., & Bellosi, A. (2001). Laser micromachining of silicon carbide. *Key Engineering Materials, 206–213*, 305–308.
102. Palma, C., & Sapia, C. (2000). Laser pattern-write crystallization of amorphous SiC alloys. *Journal of Electronic Materials, 29*(5), 607–610.
103. Reitano, R., Baeri, P., & Marino, N. (1996). Excimer laser induced thermal evaporation and ablation of silicon carbide. *Applied Surface Science, 96–98*, 302–308.
104. Shi, Y., Sun, Y., Liu, J., Tang, J., Li, J., Ma, Z., Cao, H., Zhao, R., Kou, Z., Huang, K., & Gao, J. (2018). UV nanosecond laser machining and characterization for SiC MEMS sensor application. *Sensors and Actuators, A: Physical, 276*, 196–204.
105. Desbiens, J.-P., & Masson, P. (2007). ArF excimer laser micromachining of Pyrex, SiC and PZT for rapid prototyping of MEMS components. *Sensors and Actuators A: Physical, 136*(2), 554–563.
106. Kreutz, E.-W., Weichenhain, R., & Horn, A. (2001). Nd:YAG laser micromachining of SiC precision structures for MEMS. In *Proceedings of the SPIE 4407, MEMS design, fabrication, characterization, and packaging*. SPIE.
107. Hwang, J., Cho, Y. H., Park, M. S., & Kim, B. H. (2019). Microchannel Fabrication on Glass Materials for Microfluidic Devices. *International Journal of Precision Engineering and Manufacturing, 20*(3), 479–495.
108. Kim, H. G., & Park, M. S. (2017). Circuit patterning using laser on transparent material. *Surface and Coatings Technology, 315*, 377–384.
109. Kim, H. G., & Park, M. S. (2021). Fast fabrication of conductive copper structure on glass material using laser-induced chemical liquid phase deposition. *Applied Sciences (Switzerland), 11*(18), 8695.
110. Anderson, T. J., Ren, F., Covert, L., Lin, J., Pearton, S. J., Dalrymple, T. W., Bozada, C., Fitch, R. C., Moser, N., Bedford, R. G., & Schimpf, M. (2006). Comparison of laser-wavelength operation for drilling of via holes in AlGaN/GaN HEMTs on SiC substrates. *Journal of Electronic Materials, 35*(4), 675–679.
111. Kim, B., Iida, R., Kiyokawa, S., & Fushinobu, K. (2018). Effect of beam profile on nanosecond laser drilling of 4H-SIC. *Journal of Laser Applications, 30*(3), 032207–032207.
112. Kim, S., Bang, B. S., Ren, F., D'entremont, J., Blumenfeld, W., Cordock, T., & Pearton, S. J. (2004). SiC via holes by laser drilling. *Journal of Electronic Materials, 33*(5), 477–480.
113. Deng, D., Xie, Y., Chen, L., & Chen, X. (2019). Experimental investigation on laser micromilling of SiC microchannels. *International Journal of Advanced Manufacturing Technology, 101*(1–4), 9–21.
114. Dong, Y., & Molian, P. (2003). Femtosecond pulsed laser ablation of 3CSiC thin film on silicon. *Applied Physics A: Materials Science & Processing, 77*(6), 839–846.
115. Farsari, M., Filippidis, G., Zoppel, S., Reider, G. A., & Fotakis, C. (2005). Efficient femtosecond laser micromachining of bulk 3C-SiC. *Journal of Micromechanics and Microengineering, 15*(9), 1786–1789.
116. Zoppel, S., Farsari, M., Merz, R., Zehetner, J., Stangl, G., Reider, G. A., & Fotakis, C. (2006). Laser micro machining of 3C–SiC single crystals. *Microelectronic Engineering, 83*(4–9), 1400–1402.
117. Li, W., Zhang, R., Liu, Y., Wang, C., Wang, J., Yang, X., & Cheng, L. (2016). Effect of different parameters on machining of SiC/SiC composites via pico-second laser. *Applied Surface Science, 364*, 378–387.
118. Liu, Y., Zhang, R., Li, W., Wang, J., Yang, X., Cheng, L., & Zhang, L. (2018). Effect of machining parameter on femtosecond laser drilling processing on SiC/SiC composites. *International Journal of Advanced Manufacturing Technology, 96*(5–8), 1795–1811.
119. Vendan, M., Molian, P., Bastawros, A., & Anderegg, J. (2005). Ultra-short pulsed laser deposition and patterning of SiC thin films for MEMS fabrication. *Materials Science in Semiconductor Processing, 8*(6), 630–645.
120. Huang, Y., Wu, X., Liu, H., & Jiang, H. (2017). Fabrication of through-wafer 3D microfluidics in silicon carbide using femtosecond laser. *Journal of Micromechanics and Microengineering, 27*(6), 065005.
121. Zhao, Q. Z., Ciobanu, F., Malzer, S., & Wang, L. J. (2007). Enhancement of optical absorption and photocurrent of 6H-SiC by laser surface nanostructuring. *Applied Physics Letters, 91*(12), 121107–121107.
122. Feng, S., Huang, C., Wang, J., & Zhu, H. (2017). Investigation and modelling of hybrid laser-waterjet micromachining of single crystal SiC wafers using response surface methodology. *Materials Science in Semiconductor Processing, 68*(June), 199–212.
123. Feng, S., Huang, C., Wang, J., & Jia, Z. (2018). Surface quality evaluation of single crystal 4H-SiC wafer machined by hybrid laser-waterjet: Comparing with laser machining. *Materials Science in Semiconductor Processing, 2019*(93), 238–251.
124. Dolgaev, S. I., Voronov, V. V., Shafeev, G. A., Fauquet-Ben Ammar, C., Themlin, J.-M., Cros, A., & Marine, W. (1997). Laser-induced fast etching and metallization of SiC ceramics. *Applied Surface Science, 109–110*, 559–562.
125. Bilal, A., Jahan, M. P., Talamona, D., & Perveen, A. (2019). Electro-discharge machining of ceramics: A review. *Micromachines, 10*(1), 10.

126. Schubert, A., Zeidler, H., Kühn, R., & Hackert-Oschätzchen, M. (2015). Microelectrical discharge machining: A suitable process for machining ceramics. *Journal of Ceramics, 2015*, 1–9.
127. Taki, Y., Kitiwan, M., Katsui, H., & Goto, T. (2018). Electrical and thermal properties of off-stoichiometric SiC prepared by spark plasma sintering. *Journal of Asian Ceramic Societies, 6*(1), 95–101.
128. Yan, J., & Tan, T.-H. (2015). Sintered diamond as a hybrid EDM and grinding tool for the micromachining of single-crystal SiC. *CIRP Annals, 64*(1), 221–224.
129. Tan, T.-H., & Yan, J. (2017). Atomic-scale characterization of subsurface damage and structural changes of single-crystal silicon carbide subjected to electrical discharge machining. *Acta Materialia, 123*, 362–372.
130. Kliuev, M., Maradia, U., Boccadoro, M., Perez, R., Stirnimann, J., & Wegener, K. (2016). Experimental study of EDM-drilling and shaping of SiSiC and SiC. *Procedia CIRP, 42*, 191–196.
131. Kato, T., Noro, T., Takahashi, H., Yamaguchi, S., & Arai, K. (2008). Characterization of electric discharge machining for silicon carbide single crystal. *Materials Science Forum, 600–603*, 855–858.
132. Yamamoto, N., Yamaguchi, S., & Kato, T. (2013). Slicing of rotating SiC ingot by electric discharge machining. *Materials Science Forum, 740–742*, 843–846.
133. Itokazu, A., Hashimoto, T., Fukushima, K., Yuzawa, T., & Sato, T. (2013). MULTI-wire electrical discharge slicing for silicon carbide. *Materials Science Forum, 740–742*, 841–842.
134. Kimura, A., Okamoto, Y., Okada, A., Ohya, J., & Yamauchi, T. (2013). Fundamental study on multi-wire EDM slicing of SiC by wire electrode with track-shaped section. *Procedia CIRP, 6*, 232–237.
135. Zhao, Y., Kunieda, M., & Abe, K. (2016). Challenge to EDM slicing of single crystal SiC with blade electrode utilizing a reciprocating worktable. *Procedia CIRP, 42*, 185–190.
136. Zhao, Y. H., Kunieda, M., & Abe, K. (2014). Study of EDM cutting of single crystal silicon carbide. *Precision Engineering-Journal of the International Societies for Precision Engineering and Nanotechnology, 38*(1), 92–99.
137. Liew, P. J., Yan, J., & Kuriyagawa, T. (2013). Carbon nanofiber assisted micro electro discharge machining of reaction-bonded silicon carbide. *Journal of Materials Processing Technology, 213*(7), 1076–1087.
138. Liew, P. J., Shimada, K., Mizutani, M., Yan, J., & Kuriyagawa, T. (2013). Fabrication of microstructures on RB-SiC by ultrasonic cavitation assisted micro-electrical discharge machining. *International Journal of Automation Technology, 7*(6), 621–629.
139. Liew, P. J., Yan, J., & Kuriyagawa, T. (2014). Fabrication of deep micro-holes in reaction-bonded SiC by ultrasonic cavitation assisted micro-EDM. *International Journal of Machine Tools and Manufacture, 76*, 13–20.
140. Choi, S., & Park, M. (2019). Fabrication of conductive patterns on 3D printed structure using photo-polymerization technology. *Physica Status Solidi (A) Applications and Materials Science, 216*(16), 1801017.
141. Hwang, S. R., & Park, M. S. (2021). Property analysis of photo-polymerization-type 3d-printed structures based on multi-composite materials. *Applied Sciences (Switzerland), 11*(18), 8545.
142. Shin, I. J., & Park, M. S. (2018). Direct conductive patterning on 3D printed structure using laser. *Physica Status Solidi (A), 215*(1), 1700597–1700597.
143. He, R., Zhou, N., Zhang, K., Zhang, X., Zhang, L., Wang, W., & Fang, D. (2021). Progress and challenges towards additive manufacturing of SiC ceramic. *Journal of Advanced Ceramics, 10*(4), 637–674.
144. Ortona, A., D'Angelo, C., Gianella, S., & Gaia, D. (2012). Cellular ceramics produced by rapid prototyping and replication. *Materials Letters, 80*, 95–98.
145. Rezaei, E., Barbato, M., Gianella, S., Ortona, A., & Haussener, S. (2020). Pressure drop and convective heat transfer in different SiSiC structures fabricated by indirect additive manufacturing. *Journal of Heat Transfer, 142*(3), 11.
146. Tu, T., & Jiang, G. (2018). SiC reticulated porous ceramics by 3D printing, gelcasting and liquid drying. *Ceramics International, 44*(3), 3400–3405.
147. Evans, R. S., Bourell, D. L., Beaman, J. J., & Campbell, M. I. (2005). Rapid manufacturing of silicon carbide composites. *Rapid Prototyping Journal, 11*(1), 37–40.
148. Nelson, J. C., Vail, N. K., Barlow, J. W., Beaman, J. J., Bourell, D. L., & Marcus, H. L. (1995). Selective laser sintering of polymer-coated silicon carbide powders. *Industrial & Engineering Chemistry Research, 34*(5), 1641–1651.
149. Exner, H., Horn, M., Streek, A., Ullmann, F., Hartwig, L., Regenfuß, P., & Ebert, R. (2008). Laser micro sintering: A new method to generate metal and ceramic parts of high resolution with sub-micrometer powder. *Virtual and Physical Prototyping, 3*(1), 3–11.
150. Liu, K., Wu, T., Bourell, D. L., Tan, Y., Wang, J., He, M., Sun, H., Shi, Y., & Chen, J. (2018). Laser additive manufacturing and homogeneous densification of complicated shape SiC ceramic parts. *Ceramics International, 44*(17), 21067–21075.
151. Xu, T. T., Cheng, S., Jin, L. Z., Zhang, K., & Zeng, T. (2020). High-temperature flexural strength of SiC ceramics prepared by additive manufacturing. *International Journal of Applied Ceramic Technology, 17*(2), 438–448.
152. Fleisher, A., Zolotaryov, D., Kovalevsky, A., Muller-Kamskii, G., Eshed, E., Kazakin, M., & Popov, V. V., Jr. (2019). Reaction bonding of silicon carbides by Binder Jet 3D-Printing, phenolic resin binder impregnation and capillary liquid silicon infiltration. *Ceramics International, 45*(14), 18023–18029.
153. Zocca, A., Lima, P., Diener, S., Katsikis, N., & Günster, J. (2019). Additive manufacturing of SiSiC by layerwise slurry deposition and binder jetting (LSD-print). *Journal of the European Ceramic Society, 39*(13), 3527–3533.
154. Polzin, C., Günther, D., & Seitz, H. (2015). 3D printing of porous Al_2O_3 and SiC ceramics. *Journal of Ceramic Science and Technology, 6*(2), 141–146.
155. Gómez-Gómez, A., Moyano, J. J., Osendi, M. I., Belmonte, M., & Miranzo, P. (2021). The effect of rod orientation on the strength of highly porous filament printed 3D SiC ceramic architectures. *Boletín de la Sociedad Española de Cerámica y Vidrio, 60*(2), 119–127.
156. Gómez-Gómez, A., Moyano, J. J., Román-Manso, B., Belmonte, M., Miranzo, P., & Osendi, M. I. (2019). Highly-porous hierarchical SiC structures obtained by filament printing and partial sintering. *Journal of the European Ceramic Society, 39*(4), 688–695.
157. Chen, H., Wang, X., Xue, F., Huang, Y., Zhou, K., & Zhang, D. (2018). 3D printing of SiC ceramic: Direct ink writing with a solution of preceramic polymers. *Journal of the European Ceramic Society, 38*(16), 5294–5300.
158. Wahl, L., Lorenz, M., Biggemann, J., & Travitzky, N. (2019). Robocasting of reaction bonded silicon carbide structures. *Journal of the European Ceramic Society, 39*(15), 4520–4526.
159. Ji, S. H., Kim, D. S., Park, M. S., Lee, D., & Yun, J. S. (2021). Development of multicolor 3D-printed 3Y-ZrO_2 sintered bodies by optimizing rheological properties of UV-curable high-content ceramic nanocomposites. *Materials & Design, 209*, 109981–109981.
160. Chen, J., Wang, Y., Pei, X., Bao, C., Huang, Z., He, L., & Huang, Q. (2020). Preparation and stereolithography of SiC ceramic

precursor with high photosensitivity and ceramic yield. *Ceramics International, 46*(9), 13066–13072.
161. Eckel, Z. C., Zhou, C., Martin, J. H., Jacobsen, A. J., Carter, W. B., & Schaedler, T. A. (2016). Additive manufacturing of polymer-derived ceramics. *Science, 351*(6268), 58–62.
162. Friedel, T., Travitzky, N., Niebling, F., Scheffler, M., & Greil, P. (2005). Fabrication of polymer derived ceramic parts by selective laser curing. *Journal of the European Ceramic Society, 25*(2–3), 193–197.
163. Park, S., Lee, D. H., Ryoo, H. I., Lim, T. W., Yang, D. Y., & Kim, D. P. (2009). Fabrication of three-dimensional SiC ceramic microstructures with near-zero shrinkage via dual crosslinking induced stereolithography. *Chemical Communications, 32*, 4880–4880.
164. Ding, G., He, R., Zhang, K., Zhou, N., & Xu, H. (2020). Stereolithography 3D printing of SiC ceramic with potential for lightweight optical mirror. *Ceramics International, 46*(11), 18785–18790.
165. He, R., Ding, G., Zhang, K., Li, Y., & Fang, D. (2019). Fabrication of SiC ceramic architectures using stereolithography combined with precursor infiltration and pyrolysis. *Ceramics International, 45*(11), 14006–14014.

Younghak Cho received the M.Eng. degree from the Department of Mechanical Design and Production Engineering, Seoul National University, Seoul, Korea, in 2001, and the Ph.D. degree in precision machinery engineering from The University of Tokyo, Tokyo, Japan, in 2005. From April 2005 to August 2007, he was with the Institute of Industrial Science, The University of Tokyo, as a JSPS Postdoctoral Researcher. From October 2007 to February 2009, he was with the Department of Electrical and Computer Engineering, Texas A&M University, College Station, as a Postdoctoral Research Associate. He is currently a Professor in the Department of Mechanical System Design Engineering, Seoul National University of Science and Technology. His current research interests include the development and application of microfluidic devices for cell separation and droplet generation.

Jihong Hwang got his PhD degree in Industrial Engineering at Purdue University, West Lafayette, IN, USA in 2005. He received masters' and bachelor's degrees in Mechanical Design and Production Engineering from Seoul National University, Seoul, South Korea. He is currently working as a Professor in the department of Mechanical System Design Engineering at Seoul National University of Science & Technology, Seoul, South Korea. His research interests are in the areas of Machining and Grinding Processes, Metrology and Instrumentation, and Design for Additive Manufacturing.

Min-Soo Park received his Ph.D. in Mechanical Engineering from Seoul National University in 2007. He received bachelor's degrees in Mechanical and Aerospace Engineering from Seoul National University. He is currently working as a full Professor in the department of Mechanical System Design Engineering at Seoul National University of Science and Technology, Seoul, South Korea. His research interests are metal and ceramic 3D printing, laser processing and micro machining.

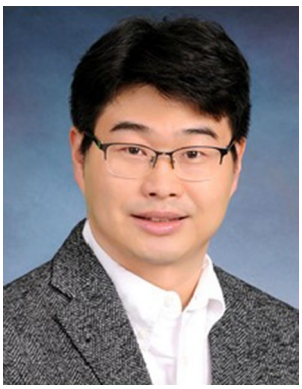

Bo Hyun Kim received his Ph.D. in Mechanical and Aerospace Engineering from Seoul National University in 2005. He received masters' and bachelor's degrees in Mechanical Design and Production Engineering from Seoul National University. He is currently working as a Professor in the School of Mechanical Engineering at Soongsil University, Seoul, South Korea. His research interests include micro machining and non-conventional machining processes.